Department of Applied Physics

# Modeling of polymer-metal hybrid materials

Janne Blomqvist

Aalto University

DOCTORAL DISSERTATIONS

Aalto University publication series
**DOCTORAL DISSERTATIONS** 114/2012

# Modeling of polymer-metal hybrid materials

**Janne Blomqvist**

Doctoral dissertation for the degree of Doctor of Science in Technology to be presented with due permission of the School of Science for public examination and debate in Auditorium TU2 at the Aalto University School of Science (Espoo, Finland) on the 11th of October 2012 at 13 o'clock.

**Aalto University**
**School of Science**
**Department of Applied Physics**
**COMP/EPM**

**Supervising professor**
Prof. Risto Nieminen

**Thesis advisor**
Doc. Petri Salo

**Preliminary examiners**
Prof. Kalevi Kokko, University of Turku, Finland
Dr. Karen Johnston, Max Planck Institute for Polymer Research, Germany

**Opponents**
Prof. Kai Nordlund, University of Helsinki, Finland

Aalto University publication series
**DOCTORAL DISSERTATIONS** 114/2012



ISBN 978-952-60-4774-4 (printed)
ISBN 978-952-60-4775-1 (pdf)
ISSN-L 1799-4934
ISSN 1799-4934 (printed)
ISSN 1799-4942 (pdf)
http://urn.fi/URN:ISBN:978-952-60-4775-1

Unigrafia Oy
Helsinki 2012

Finland

441 697
Printed matter

Aalto University

# Abstract

Aalto University, P.O. Box 11000, FI-00076 Aalto www.aalto.fi

**Author**
Janne Blomqvist

**Name of the doctoral dissertation**
Modeling of polymer-metal hybrid materials

**Publisher** School of Science

**Unit** Department of Applied Physics

**Series** Aalto University publication series DOCTORAL DISSERTATIONS 114/2012

**Field of research** Computational Physics

**Manuscript submitted** 12 June 2012 **Date of the defence** 11 October 2012

**Permission to publish granted (date)** 16 August 2012 **Language** English

☐ **Monograph** ☒ **Article dissertation (summary + original articles)**

**Abstract**

Hybrid materials, where multiple substances are combined, belong to an interesting new class of materials. These materials can be optimized for specific applications and can provide a more appropriate balance between cost, weight, strength, or some other properties. Particularly interesting materials from a practical as well as a scientific perspective are the materials that combine a polymer with a metal. To understand these materials we must understand how the various substances interact with each other.

In this thesis I have studied the interaction between a polymer and a metal surface at the microscopic level. I have used density-functional theory (DFT) and coarse-grained molecular dynamics to study the binding between the polymer and the metal surface. In order to provide a more realistic description for the binding of these substances I have taken into account van der Waals (vdW) interactions within DFT.

My results suggest that the polymer-metal binding can be strongly affected by small amounts of doping at the interface, thus providing one way to tune the polymer-metal interface properties. Also, the vdW interaction plays a major role, and it is thus essential to include these effects when studying large molecules on surfaces. I have used the DFT results to parametrize interaction potentials for coarse-grained molecular-dynamics simulations, which I have used to study the hybrid material interface on a larger length and time scale. A hybrid simulation method which combines molecular dynamics and continuum dynamics in the same system, allows the study of even larger systems. The hybrid simulation method can also be used to equilibrate the polymer system faster than with traditional methods.

Computer simulations offer the possibility to efficiently test the properties of various material combinations before committing to produce physical manifestations of these materials. These simulations can be used for providing e.g. effective boundary conditions such as friction coefficients that can be used for continuum simulations, or for simulating nanostructured composites where the interface effects dominate the bulk properties of the material.

**Keywords** polymer, surface, density-functional theory, molecular dynamics

**ISBN (printed)** 978-952-60-4774-4 **ISBN (pdf)** 978-952-60-4775-1

**ISSN-L** 1799-4934 **ISSN (printed)** 1799-4934 **ISSN (pdf)** 1799-4942

**Location of publisher** Espoo **Location of printing** Helsinki **Year** 2012

**Pages** 111 **urn** http://urn.fi/URN:ISBN:978-952-60-4775-1

Aalto-universitetet

# Sammandrag

**Aalto-universitetet, PB 11000, 00076 Aalto** www.aalto.fi

**Författare**
Janne Blomqvist

**Doktorsavhandlingens titel**
Simulering av polymer-metall hybridmaterial

**Utgivare** Högskolan för teknikvetenskaper

**Enhet** Institutionen för teknisk fysik

**Seriens namn** Aalto University publication series DOCTORAL DISSERTATIONS 114/2012

**Forskningsområde** Beräkningsfysik

**Inlämningsdatum för manuskript** 12.06.2012 **Datum för disputation** 11.10.2012

**Beviljande av publiceringstillstånd (datum)** 16.08.2012 **Språk** Engelska

☐ **Monografi** ☒ **Sammanläggningsavhandling (sammandrag plus separata artiklar)**

**Sammandrag**

Hybridmaterial är en ny klass av material där flera olika substanser kombineras. Dessa material kan optimeras för specifika tillämpningar, och kan ge en bättre balans mellan vikt, styrka, kostnad, och andra egenskaper. Speciellt intressanta hybridmaterial både ur en praktisk och en vetenskaplig synvinkel är material där man kombinerar en polymer med en metall eller metalloxid. För att förstå dessa nya material måste man förstå hur de olika substanserna växelverkar.

I denna avhandling har vi studerat växelverkan mellan en polymer och en metallyta på mikroskopisk nivå. Vi har använt täthetsfunktionalteori (DFT) samt grovkorning molekyldynamik för att studera bindningen mellan en polymerkedja och en metallyta. För att tillhandahålla en mer realistisk beskrivning för bindningen av dessa substanser tar vi också hänsyn till van der Waals växelverkan inom DFT.

Våra resultat tyder på att polymer-metall-bindningen starkt kan påverkas av små mängder av dopning vid gränsytan, vilket ger ett sätt att optimera polymer-metall-gränsytans egenskaper. Dessutom spelar vdW-växelverkan en viktig roll, och det är därför viktigt att inkludera dessa effekter när man studerar stora molekyler på ytor. Vi har använt våra DFT resultat till att parametrisera interaktionspotentialer för grovkorniga molekyldynamiksimuleringar, som vi använt för att studera hybridmaterial-gränssnittet över en större längd- och tidsskala. En hybrid-simuleringsmetod som kombinerar molekyldynamik och kontinuumdynamik i samma system möjliggör studier av ännu större system. Hybridmetoden kan också användas för att jämvikta polymersystemet snabbare än traditionella metoder.

Datorsimuleringar ger möjlighet att effektivt testa egenskaperna hos olika materialkombinationer innan man bestämmer sig för att producera fysiska manifestationer av dessa material. Dessa simuleringar kan användas för att tillhandahålla t.ex. gränsvillkor såsom friktionskoefficienter som kan användas för kontinuumsimuleringar, eller för simulering av nanostrukturerade kompositer där gränssnittets egenskaper dominerar materialets bulkegenskaper.

**Nyckelord** polymer, ytor, täthetsfunktionalteori, molekyldynamik

**ISBN (tryckt)** 978-952-60-4774-4 **ISBN (pdf)** 978-952-60-4775-1

**ISSN-L** 1799-4934 **ISSN (tryckt)** 1799-4934 **ISSN (pdf)** 1799-4942

**Utgivningsort** Esbo **Tryckort** Helsingfors **År** 2012

**Sidantal** 111 **urn** http://urn.fi/URN:ISBN:978-952-60-4775-1

# Preface

The work presented in this thesis has been conducted in the COMP Center of Excellence in Computational Nanoscience at the Department of Applied Physics, Aalto University School of Science.

I wish to express my gratitude to my instructor Docent Petri Salo and my supervisor Aalto Professor Risto Nieminen for patient support and guidance during these years. I also thank my current and former colleagues for invaluable scientific discussions, in particular Karen Johnston, Yasuhiro Senda, and Andris Gulans.

This research has been supported through the TEKES Hypris and K3MAT projects. I would like to thank all my coworkers from those two projects. The computer simulations in this thesis have been performed with local resources as well as those of IT Center for Science Ltd. (CSC).

Finally, I wish to thank my family and friends.

Helsinki, September 7, 2012,

Janne Blomqvist

# Contents

# List of Publications

This thesis consists of an overview and of the following publications which are referred to in the text by their Roman numerals.

**I** Janne Blomqvist, Lauri Lehman, and Petri Salo. CO adsorption on metal-oxide surfaces doped with transition-metal adatoms. *Physica Status Solidi B*, 249, 1046, May 2012.

**II** Janne Blomqvist and Petri Salo. Adsorption of benzene, phenol, propane and carbonic acid molecules on oxidized Al(111) and $\alpha$-$Al_2O_3$(0001) surfaces: A first-principles study. *Journal of Physics: Condensed Matter*, 21, 225001, April 2009.

**III** Janne Blomqvist and Petri Salo. First-principles study for the adsorption of segments of BPA-PC on $\alpha$-$Al_2O_3$(0001). *Physical Review B*, 84, 153410, October 2011.

**IV** Yasuhiro Senda, Miyuki Fujio, Shuji Shimamura, Janne Blomqvist, and Risto M. Nieminen. Fast convergence to equilibrium for long-chain polymer melts using a MD/continuum hybrid method. *Accepted with changes in Journal of Chemical Physics*, arXiv:1205.6582, 2012.

# Author's Contribution

**Publication I: "CO adsorption on metal-oxide surfaces doped with transition-metal adatoms"**

The author did the majority of the calculations and has been the main writer.

**Publication II: "Adsorption of benzene, phenol, propane and carbonic acid molecules on oxidized Al(111) and $\alpha$-$Al_2O_3$(0001) surfaces: A first-principles study"**

The author did all the calculations and has been the main writer.

**Publication III: "First-principles study for the adsorption of segments of BPA-PC on $\alpha$-$Al_2O_3$(0001)"**

The author did all the calculations and has been the main writer.

**Publication IV: "Fast convergence to equilibrium for long-chain polymer melts using a MD/continuum hybrid method"**

The author has contributed to the planning of the calculations and to the development of the computer codes. He has also contributed to the writing of the manuscript.

Additionally, Section 4.3 in this thesis contains new and original results not published elsewhere.

# 1. Introduction

Hybrid materials, where multiple substances are combined, belong to an interesting new class of materials. These materials can be optimized for specific applications and can provide a more appropriate balance between cost, weight, strength, or some other properties. To understand these materials we must understand the behavior of the interface between the various substances.

Particularly interesting materials from a practical as well as a scientific perspective are the materials that combine a metal and polymer. Depending on the applications, these materials may be manufactured in different ways. For instance, a polymer melt may be injection molded into a mold where the metal part is already present, or pre-fabricated metal and polymer parts can be assembled together with the help of some additional binding agent such as various glues. Thus, studying the interaction between a metal surface and molecules in the polymer chains is important. There are multiple adhesion mechanisms that need to be understood, such as mechanical gripping, and multiple phenomena affecting the strength of the interface, such as the surface roughness and wetting. However, in this work we have focused on the microscopic level.

We use density-functional theory (DFT) calculations to study the binding between fragments of the polymer chain and the oxide surface. We study how changes to the surface, such as oxidization or addition of small amounts of transition metals change the binding mechanism. For studying the interaction of large polymer fractions with the surface, we use DFT together with van der Waals corrections in order to calculate more accurate binding energies for these large molecules. These results are used to parametrize interaction potentials for coarse-grained molecular-dynamics simulations which we use to study the properties of the hybrid material interface on a larger length and time scale than possible with atomistic molecular dynamics. Such simulations could be used for providing e.g. boundary conditions such as friction coefficients that can be used in continuum simulations or for simulating nanostructured composites

where the interface effects dominate the bulk properties of the material.

Going further towards the macroscopic world, we combine the coarse-grained molecular-dynamics approach with a continuum mechanics model. This allows the concurrent coupling of the different regions, mediated by a boundary layer, where the continuum system creates an external pressure on the MD simulation box, and vice versa. In our case, we use this hybrid model to equilibrate the polymer melt quicker than what would otherwise be possible. Equilibration of polymer melts is a significant problem for simulations, as the entangled polymer chains cause the dynamics to be very slow. In the hybrid approach, large pressure and volume fluctuations in the continuum system affect the MD system and helps the MD system overcome energy barriers, thus leading to faster equilibration.

# 2. Hybrid materials

By combining several materials one can produce hybrid materials which combine the strengths of the constituent materials and avoid typical downsides. Due to this, hybrid materials have become a new and interesting subfield of materials science. Traditional single-component materials such as polymers, metals, and ceramics can be combined in various ways. One can also add specific substances such as chemical functional groups or even molecules of biological origin, in order to functionalize a material or to allow structures to be built bottom-up in a building-block approach such as molecular self-assembly.

Once the dimensions of the constituent materials in a hybrid material become small enough, one can talk of nanocomposites. These can be distinguished by the fact that at a small scale, the surface effects at the interfaces start to dominate the bulk properties of the constituent materials. Essentially this is due to the surface-to-volume ratio of the system, including internal interfaces between the constituent materials, becoming larger as the dimensions of the components become smaller.

## 2.1 Plastic-metal hybrid materials

When combining a plastic material and a metal, the constituent materials can provide advantages such as [Hoikkanen et al., 2008]:

**Plastic**

- Complex design opportunities
- High integration capability
- Chemical and corrosion resistance

- Bulk coloring
- Weight saving compared to an all-metal counterpart

**Metal**

- Higher modulus of elasticity
- Rigidity
- Stiffness

For instance, enclosing a fiber reinforced plastic (FRP) material with thin metal sheets can prevent moisture accumulation in the FRP which is important for lightweight structures.

The introduction of hybrid materials enables new dimensions in the materials design space, considering the different constituent materials that can be chosen, how they are bound to each other, and how they can be manufactured. Thus, in order to design an optimal material for a particular application, one needs to optimize a large number of parameters. In essence, one needs a systematic understanding of how the various material and parameter choices influence the properties of the hybrid material. The hope is that computer simulations will eventually be able to drastically reduce the amount of work involved in testing different parameter combinations.

Plastic-metal hybrid materials can be produced with a variety of processing methods such as injection molding or by gluing together pre-fabricated elements. If possible, injection molding is often preferred as it enables faster fabrication by skipping the assembling and gluing step. A schematic overview of a basic injection molding machine can be seen in Fig. 2.1. In the injection molding process, plastic granules are introduced into the hopper which feeds the granules into the barrel. Inside the barrel, a reciprocating screw propels the granules forward along the barrel. The barrel is heated, causing the plastic granules to melt, thus forming a polymer melt, a highly viscous liquid. The screw then forces the molten plastic through the nozzle at high pressure into the mold cavity, where the plastic is then cooled down and allowed to solidify. Finally, the mold is opened and the finished plastic component is removed.

In order to bind together the plastic and metal in the injection molding process, one can either rely on the polymer melt directly binding to the metal sur-

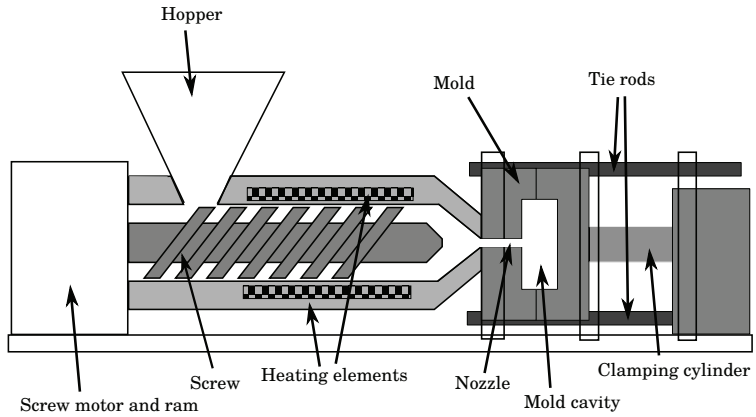


**Figure 2.1.** Schematic figure of an injection molding machine.

face or perform various kinds of pre-treatments of the metal insert in order to enhance the binding. For cost reasons, direct binding is preferable, however, depending on the materials in question the binding may be too weak. In particular, the thermal expansion coefficients are typically very different for the polymer and the metal parts, and as the components cool down after the injection molding procedure, large shear stresses form at the interface. Typical thermal expansion coefficients for plastics are a factor of 4-8 larger than for metals, whereas for ceramics up to a factor of 100 differences are possible. For polymers which are above the rubber-glass transition temperature this may not be a problem, as the polymer is flexible, but for a polymer which is in the glass or crystalline phase, this may lead to delamination. In such cases one can use a rubbery interface material between the metal and the bulk polymer, which allows the shear stresses to relax in the rubber material. Use of such interface materials has been extensively studied in the Hypris [Hoikkanen et al., 2008] and K3MAT [Luukkonen et al., 2011] projects. In general, the rubbery interface materials do avoid the issue of delamination due to thermal stress, but bring their own problems such as durability during repeated stress cycling. Another method for reducing the problem of mismatched thermal expansion coefficients is to use a *filler* material, which is a material with a low thermal expansion coefficient (e.g. glass) and which is blended into the polymer mass in granular form. On the other hand, using a filler material will reduce the strength of the polymer, both the internal strength of the bulk and the interfacial strength in a hybrid composite.

Also, if a metal insert is present in the mold during the injection of the polymer mass, discontinuities and stress concentrations form. This has to be taken care of during the design process. Typically, choosing a rounded geometry for

the metal insert as well as pre-heating of the insert will reduce the stress development.

## 2.2 Examples of hybrid materials

A common class of hybrid materials are fiber-metal laminates (FML) [Vermeeren, 2003, Sinmazçelik et al., 2011]. They consist of layers of metal and fiber-reinforced plastic. Depending on the application, either a thermoset or a thermoplastic can be used for the plastic component, although so far all commercially available FML's are based on thermosets. In hybrid materials, the choice of reinforcing fibers is also affected by compatibility with the chosen metal, such that one tries to minimize stresses in the material due to thermal expansion. The thickness of the layers is usually 1-10 mm. The thickness and the number of layers depend on the application. Also the direction of the reinforcing fibers can be directed in order to optimize the strength and stiffness properties along some specific direction in the laminate.

As an example of an FML, GLARE (GLAss REinforced) is one of the more widely publicised ones [Vermeeren, 2003, Botelho et al., 2006, Sinmazçelik et al., 2011]. It is a sandwich of aluminium and pre-impregnated (prepreg) glass fiber reinforced epoxy, developed in the 1980's at Delft University of Technology. An exploded view of the laminate can be seen in Fig. 2.2. So far, GLARE has been used mainly in the aerospace industry, e.g. upper fuselage panels on the Airbus A380 and blast resistant luggage containers. The main advantage of the material, compared to traditional aluminium construction, is improved resistance to fatigue stress, as the flexible fiber/epoxy layers prevent microscopic stress induced cracks in the metal from propagating. Also, impact properties are significantly improved compared to aluminium or fiber laminates only. Modeling and characterization work of this material has also been done as part of the K3MAT project [Luukkonen et al., 2011]. There are 6 different grades of the material which have been characterized and are available commercially, differing in the thickness of the metal sheets, the used aluminium alloys, and direction of the reinforcing fibers in the prepreg. The cost of GLARE has been estimated to be about 5 to 10 times more expensive per kilogram than traditional aluminium alloys used in aircraft construction. However, due to the advantageous fatigue properties of GLARE, manufactured structures can be made simpler as there is no need for reinforcements around joints and crack stoppers compared to traditional aluminium construction. Thus, when considering the total cost of a structure, a GLARE structure can come close to the cost of the equivalent

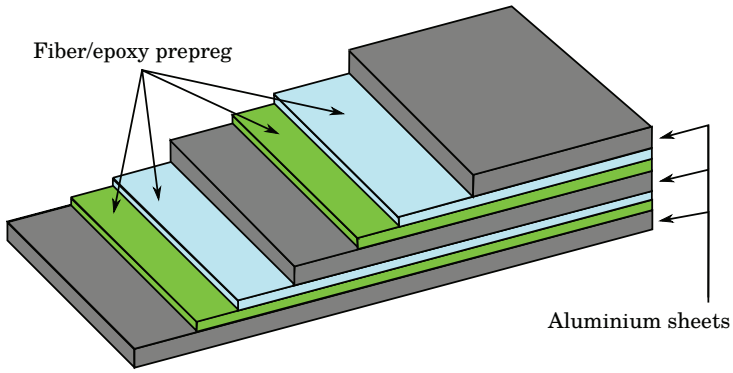


**Figure 2.2.** Configuration of the GLARE hybrid fiber metal laminate.

aluminium structure [Vermeeren, 2003].

In addition to GLARE, there are a few other FML in use. Probably the most widely used one is Arall (Aramid Reinforced Aluminium Laminates), where the layers consist of aluminium and aramid fiber reinforced epoxy, compared to GLARE where glass fibers are used instead of aramid. However, in the aerospace industry Arall has not been as successful as GLARE for structural components. Arall turned out to have relatively poor blunt notch strength, that is, strength reduction due to holes drilled into the material. A variant of Arall, Carall (Carbon reinforced aluminium laminates), uses carbon fibers instead of aramid for the reinforcing fibers in the laminate [Botelho et al., 2006, Sinmazçelik et al., 2011]. Also, many other material combinations are under active research, e.g. steel with carbon fiber prepregs, aluminium with boron fiber epoxy, titanium with carbon fiber epoxy, and so on.

In addition to FML's, other examples of hybrid materials are e.g. steel-rubber-steel structures [Luukkonen et al., 2011], which are laminates consisting of steel outer layers with rubber in-between. The main usage of such materials are for shock absorbing materials that are needed e.g. for buildings in earthquake-prone areas, sound adsorption, and other similar applications. For vibration damping applications an issue is internal heat generation due to the internal friction inside the rubber material, which can lead to overheating and subsequent material failure. Steel-plastic-steel structures are materials consisting of steel and plastic layers. Due to lacking fiber reinforcements as in FML's, these materials lack the strength and durability of FML's, but the advantage is lower production cost. The main applications of steel-plastic-steel structure have so far been in the automotive industry, where the balance between cost and weight is very different than in the aerospace industry where FML's have found their biggest success.

# 3. Methods

In this section an overview of the methods is presented. As in particular the density-functional theory (Section 3.1.1) has been extensively studied and described in the past, the overview is by necessity brief. For a more thorough description, see e.g. [Martin, 2004].

## 3.1 The electronic structure problem

Many interesting properties of condensed matter systems can be derived from the electronic structure. The basic electronic-structure problem that one tries to solve in computational condensed-matter physics is the many-body Schrödinger equation

$$\hat{H}\Psi = E\Psi\,,$$

with the Hamiltonian

$$\hat{H} = \sum_i \frac{\hat{\mathbf{p}}_i^2}{2m} + \sum_I \frac{\hat{\mathbf{P}}_I^2}{2M_I} - \sum_{i,I} \frac{Z_I e^2}{|\mathbf{r}_i - \mathbf{R}_I|}$$

$$+ \frac{1}{2}\sum_{i\neq j} \frac{e^2}{|\mathbf{r}_i - \mathbf{r}_j|} + \frac{1}{2}\sum_{I\neq J} \frac{Z_I Z_J e^2}{|\mathbf{R}_I - \mathbf{R}_J|}\,,$$

where the upper case letters and indexes indicate the ions and the lower case letters and indexes indicate the electrons. The first two terms are the kinetic energy of the electrons and the ions, respectively, the third term is the interaction between the electrons and the ions, and the last two terms are the electron-electron and ion-ion interaction terms.

This problem cannot be solved exactly for more than two particles and hence various approximations must be made in order to make the problem tractable. One approximation is to consider the electronic and ionic problems separately, as the ions are much heavier than the electrons and thus their dynamics is much slower; this is the so-called Born-Oppenheimer approximation [Born and Oppenheimer, 1927]. However, after this approximation, and even before we

start to consider how to solve the problem, we have a many-body wavefunction $\Psi(r_1,...,r_N)$ which requires exponentially large amounts of storage as $N$ increases, to the extent that even for a comparatively modest system with 1000 electrons with an accuracy of 3 bits per variable, we would need approximately $10^{1500}$ bits of storage, which can be compared to the estimated amount of baryons in the known universe, approximately $10^{80}$ [Kohn, 1999]. It is thus clear that in order to solve the electronic-structure problem for anything but the smallest systems, we need much more drastic approximations.

### 3.1.1 Density-functional theory

In order to work around the issues with the full many-body problem, as described in the preceding section, a common approach is to replace the many-body problem with a set of single-body problems where each electron moves in an effective potential created by all the other electrons in the system. The density-functional theory (DFT) is such an approach, replacing the many-body problem with the electronic density $n(\mathbf{r})$ and a set of single-particle wave functions. DFT was developed starting in 1964 when Hohenberg and Kohn [Hohenberg and Kohn, 1964] proved that there is a unique relationship between the ground-state electron density of an N-electron system and the external potential acting on it. That is, if one knows the external potential, one can construct the unique ground-state density of the electrons. From this it follows that the ground-state energy is a functional of the density. A practical approach for calculating the ground-state energy was proposed by Kohn and Sham (KS) [Kohn and Sham, 1965] in 1965, where the problem was reformulated as a mean-field theory where one iteratively solves a set of single-electron equations. In the KS approach one solves the KS equations

$$\left[-\frac{\hbar^2}{2m_e}\nabla^2 + V_{eff}\right]\phi_i(\mathbf{r}) = \epsilon_i(\mathbf{r})\phi_i(\mathbf{r})$$

$$n(\mathbf{r}) = \sum_i^N |\phi_i(\mathbf{r})|^2,$$

where $\phi_i$'s are auxiliary one-electron orbitals fulfilling the property that all the orbitals reproduce the total density $n(\mathbf{r})$. The effective potential is

$$V_{eff} = V_{ext}(\mathbf{r}) + V_H[n] + V_{xc}[n],$$

where the first term is the external potential and the last two terms are the functional derivatives with respect to the density of the Hartree energy and the exchange-correlation energy, respectively. In the Born-Oppenheimer approximation, the external potential $V_{ext}$ is the potential of the atomic nuclei. The

Hartree potential, or the Coulomb interaction between the electrons, is

$$E_H[n(\mathbf{r})] = \frac{1}{2}\int d^3\mathbf{r}d^3\mathbf{r}'\frac{n(\mathbf{r})n(\mathbf{r}')}{|\mathbf{r}-\mathbf{r}'|},$$

and the exchange-correlation energy is the part that essentially contains the many-body physics,

$$E_{xc}[n(\mathbf{r})] = \int d\mathbf{r}n(\mathbf{r})\epsilon_{xc}([n(\mathbf{r})],\mathbf{r}).$$

Thus, the effective potential can be written, in the local density approximation (LDA), as

$$\begin{aligned} V_{eff} &= V_{ext}(\mathbf{r}) + V_H[n] + V_{xc}[n] \\ &= V_{ext}(\mathbf{r}) + \frac{\delta E_H[n]}{\delta n(\mathbf{r})} + \frac{\delta E_{xc}[n]}{\delta n(\mathbf{r})} \\ &= V_{ext}(\mathbf{r}) + \int d\mathbf{r}'\frac{n(\mathbf{r}')}{|\mathbf{r}-\mathbf{r}'|} \\ &\quad + \epsilon_{xc}([n(\mathbf{r})],\mathbf{r}) + n(\mathbf{r})\frac{\delta\epsilon_{xc}([n(\mathbf{r})],\mathbf{r})}{\delta n(\mathbf{r})}. \end{aligned}$$

Beyond the LDA, one can improve the accuracy of the calculation by including other properties than the local electron density in the expression for the exchange-correlation energy. In this thesis all DFT calculations have been done with the generalized gradient approximation (GGA), where in addition to the density also the gradient of the density is taken into account. The exchange-correlation energy is thus of the form

$$E_{xc}^{GGA}[n(\mathbf{r})] = \int f(n(\mathbf{r}),\nabla n(\mathbf{r}))d\mathbf{r},$$

where $f$ is a function of both the density and its gradient. In the GGA, there is some freedom in how to parametrize the functional, and many different versions have been developed over the years. In this thesis, the Perdew-Wang 91 (PW91) [Perdew et al., 1992] and two revised versions of the Perdew-Burke-Ernzerhof (PBE) [Perdew et al., 1996, 1997], namely revPBE [Zhang and Yang, 1998] and RPBE [Hammer et al., 1999], have been used.

### 3.1.2 van der Waals interactions

The standard implementations of DFT do not include van der Waals (vdW) interactions, which arise due to the dynamical dipole-dipole interactions between charges. Traditionally this has not been a problem as DFT has been used, for various reasons, mostly for covalently bound or metallic systems. However, as the use of DFT has expanded to simulating large molecules such as

biomolecules, polymers, and carbon nanostructures, the lack of vdW interactions has become an acute problem. Fortunately, thanks to recent developments [Dion et al., 2004, 2005, Thonhauser et al., 2007, Román-Pérez and Soler, 2009] this problem has, to some extent, been resolved, although the various functionals are not as well tested on a wide range of systems as the plain GGA's.

Dion and coworkers [Dion et al., 2004, 2005] introduced a non-local functional which approximated the vdW interaction in terms of a density-density formulation. In DFT, we can split the exchange-correlation functional into two additive parts, one for the exchange and the other for the correlation, i.e.

$$E_{xc}[n] = E_x[n] + E_c[n].$$

In the vdW-DF approach, one usually uses a normal GGA exchange functional, revPBE [Zhang and Yang, 1998] in the original implementation, although other functionals have also been used subsequently. The correlation functional can be further split into a local and a non-local part. The local part is the plain LDA correlation, whereas the non-local part then contains the actual vdW interaction, i.e.

$$E_c[n] = E_c^{LDA}[n] + E_c^{nl}[n].$$

The non-local correlation functional is a double integral over the spatial coordinates

$$E_c^{nl}[n] = \frac{1}{2}\int d^3r \int d^3r' n(\mathbf{r})\Phi(\mathbf{r},\mathbf{r}')n(\mathbf{r}'), \tag{3.1}$$

where the kernel $\Phi$ depends on the densities and gradients as well as the distance between the points $r_{12} = |\mathbf{r} - \mathbf{r}'|$. That is,

$$\Phi(\mathbf{r},\mathbf{r}') = \Phi(q_0(\mathbf{r}), q_0(\mathbf{r}'), r_{12}),$$

where $q_0$ depends on the density and gradient at a point,

$$q_0(\mathbf{r}) = q_0(n(\mathbf{r}), |\nabla n(\mathbf{r})|).$$

While an exact form for the kernel $\Phi$ is unknown, some properties that it must fulfill are known. For a system with homogeneous density, $E_c^{nl}$ must be zero, and for large $r_{12}$ the interaction must have the $r^{-6}$ dependence that the vdW theory predicts.

Unfortunately, the double integral in Eq. (3.1) is expensive to evaluate, scaling as $O(N^2)$ in the number of charge density grid points $N$. For practical calculations, such a direct evaluation of the non-local correlation will dominate the total computation time for a DFT calculation. One way to reduce the scaling of this calculation, proposed in Ref. [Román-Pérez and Soler, 2009], is to

expand and factorize $\Phi$ as

$$\Phi(q_1, q_2, r_{12}) \approx \sum_{\alpha\beta} \Phi(q_\alpha, q_\beta, r_{12}) p_\alpha(q_1) p_\beta(q_2),$$

where $q_1 = q_0(\mathbf{r})$ , $q_2 = q_0(\mathbf{r}')$, $r_{12} = |\mathbf{r} - \mathbf{r}'|$, and $p$ is a set of cubic spline interpolation polynomials. In each of the summation terms the $q_\alpha$ in the kernel $\Phi$ are fixed values. With these changes $E_c^{nl}$ can now be seen as a convolution, which can be evaluated e.g. with the help of a Fast Fourier Transform (FFT), resulting in $O(N \log N)$ scaling. This makes it practical to perform vdW-DF calculations with a small overhead compared to plain GGA, for large systems typically in the single-digit percent range. This approach has been used in Publication III.

An alternative to the convolution-based vdW-DF algorithm described above is to evaluate $E_c^{nl}$ in real space, however by using radial atom-centered grids [Gulans et al., 2009] instead of the Cartesian grids used in the original brute-force approach. Together with a suitable cutoff for the interaction range this method can achieve $O(N)$ scaling, although the prefactor is quite large. The use of adaptive grids where the radial part can be scaled according to the scale of the kernel function as well as changing the density of the angular grid at different ranges from the nuclei, can allow the method to be very efficient for large systems.

As the vdW-DF method is still a relatively recent development, much work is going on to optimize the choice of the functional. A relatively minor change is to use the RPBE exchange instead of revPBE, giving RPBE-vdW [Moses et al., 2009, Wellendorff et al., 2010]. As the changes between RPBE and revPBE are very small, the results are also very similar. A more significant departure from the original vdW-DF approach is the vdW-DF2 functional [Lee et al., 2010]. In vdW-DF2 the revPBE exchange is replaced with a refitted PW86 [Perdew and Yue, 1986, Murray et al., 2009]. Here the choice of PW86 is motivated by the fact that the PW86 exchange very closely resembles the exact Hartree-Fock exchange. The matching of the exact Hartree-Fock exchange is usually not seen as very important for normal GGA functionals, as it is well known that one of the keys to the success of the DFT method is the cancellation of errors between the exchange and correlation functionals, particularly at longer ranges. However, in the vdW-DF method, the non-local correlation functional should fully account for the long-range interactions, and thus it is important to avoid spurious exchange binding at long range. Hence approximating the exact HF exchange becomes a valid criterion in the context of vdW-DF. Another recent vdw-DF type functional by Vydrov and van Voorhis (VV10) [Vydrov and Van Voorhis, 2010] also uses the refitted PW86 exchange, however instead of the

LDA correlation functional they use the correlation function from PBE [Perdew et al., 1996, 1997]. Also the construction of the non-local correlation functional in VV10 differs from the original vdW-DF approach, although the principles are the same. Comparisons among different vdW-DF approaches can be seen e.g. in [Björkman et al., 2012]. Finally, it is worth mentioning that a semi-empirical approach for finding inter-atomic $C_{6AB}$ coefficients for a post-hoc vdW correction to a normal GGA calculation has also been met with some success [Tkatchenko and Scheffler, 2009].

For some further examples of vdW-DF applications in addition to Publication III, see e.g. Refs. [Pakarinen et al., 2009, Johnston et al., 2010, Mura et al., 2010, Gulans et al., 2011].

### 3.1.3 Numerical approaches to solving the Kohn-Sham equations

In order to solve the electronic-structure problem in practice, one needs a numerical approach to solve the equations in the preceding sections. The wavefunctions need to be expanded in terms of a set of basis functions. In electronic-structure simulation programs, the choice has usually been either a plane-wave basis or a basis consisting of atom-centered orbital functions. More recently, representing the wave functions on a regular real-space grid and using multigrid solvers, have also been used successfully [Mortensen et al., 2005, Enkovaara et al., 2010].

In both the plane-wave and uniform real-space grid approach, an issue is that close to the atomic cores the wave functions vary rapidly, necessitating a very dense grid. On the other hand, such a dense grid is wasteful in the areas between the atoms where the wave functions vary relatively slowly. In order to allow coarser grids to be used in the inter-atomic regions, various approaches have been developed, for instance pseudopotentials [Phillips and Kleinman, 1959]. In the pseudopotential approach the rapidly varying wavefunctions in the core regions is replaced by a smoothly varying pseudo wavefunction which can thus be represented on a much coarser grid. In order to maintain the total charge in the system, many pseudopotential methods impose a norm-conservation requirement, where the norm of the pseudo wavefunctions and the corresponding all-electron wavefunctions must be equal. In Publication III we have used such a norm-conserving pseudopotential of the Troullier-Martins type [Troullier and Martins, 1991].

In Publications I-III in this thesis, we have used the projector-augmented wave (PAW) method [Blöchl, 1994], which is an approximation where the total wavefunction is summed from smoothly varying pseudo wavefunctions and

atom-centered core wavefunctions which are frozen. The expression for the wavefunction can be written as

$$\Psi = \tilde{\Psi} + \sum_i c_i(\phi_i - \tilde{\phi}_i),$$

where $\tilde{\Psi}$ is a smoothly varying pseudo wavefunction, $\phi_i$ is the all-electron wavefunction centered at ion $i$, and $\tilde{\phi}_i$ is the corresponding pseudo wavefunction in the region surrounding ion $i$. The PAW method has become very successful, as the computational performance is close to advanced pseudopotential approaches such as ultrasoft pseudopotentials [Vanderbilt, 1990], while the inclusion of the core electrons, albeit frozen, avoids some problems that the pseudopotential approach suffers from.

Another common approach is to use a set of basis functions centered on the ions. In the simplest form, this approach is the so-called linear combination of atomic orbitals (LCAO) method, where the total wavefunction is a superposition of the individual atomic orbitals. For more advanced methods, the LCAO method is often used as the starting point for further calculations. Atom-centered basis functions have the advantage that the radial dependency can be taken into account without needing a very large basis set. Basis sets can be based e.g. on suitable analytical properties, such as Gaussian-type orbitals (GTO) as is commonly used in quantum chemistry, or they can be constructed from tabulated potentials. In Publication III we have used such numerical atomic orbitals for the initial phase of the simulations.

## 3.2 Charges on atoms

For analyzing chemical binding it is sometimes useful to study the charge on the atoms and to see how these charges change as a result of a reaction. However, except for a purely ionic or purely covalent bond, this assignment of charge to atoms is not precisely defined and, thus, several methods exist, each defining the charge on an atom in a different way. An overview of some common methods can be seen in Ref. [Fonseca Guerra et al., 2004]. Generally, there are two main classes of such algorithms. The first extracts the charge from the electronic orbitals and the other uses the total charge density. In the orbital approach, the simplest case is the so-called Mulliken charges, where the charge on an atom is determined by summing the charge on all the orbitals belonging to the atom. The Mulliken charge approach is thus usable only for calculations using atom-centered basis functions. However, if the charge on an atom is calculated from the total charge density rather than the orbitals, arbitrary basis sets can

be used. In approaches using the total charge density, the most popular one is probably the Bader charge approach, which we have used in Publication I.

### 3.2.1 Bader charges

The Bader charge method [Bader, 1990] is one popular way of assigning electronic charge to atoms. The approach is based on dividing the simulation volume into subvolumes belonging to each atom. The division between the different subvolumes is done by finding the surface of minimum charge density surrounding each atom. While this definition of the atomic charge is intuitive, it is known to make bonds appear to have more ionic character than what they in reality have [Fonseca Guerra et al., 2004]. However, the results are usually correct at least qualitatively, and careful investigation of the changes in the Bader charge before and after a chemical reaction can still bring valuable insight into how the charges of the reactants change. This is useful e.g. when studying reactions on insulating surfaces, where charge effects are often of crucial importance. The Bader charge can be computed efficiently by using a grid-based method by Henkelman et al. [Henkelman et al., 2006, Sanville et al., 2007, Tang et al., 2009].

### 3.2.2 Vibrational frequencies

The change in the vibrational frequencies of an atom or molecule as it undergoes a reaction is used as an experimental tool to study various chemical reactions. For the case of surface reactions, the change in the vibrational frequencies between a molecule in vacuum and adsorbed on a surface can give information about the adsorption state.

### 3.2.3 Using CO as a probe of surface charge

The binding mechanism of carbon monoxide (CO) to a metal is traditionally described in terms of the Blyholder mechanism [Blyholder, 1964] as follows. The orbitals of the CO molecule in terms of molecular orbital theory can be seen in Fig. 3.1. When the CO molecule binds to a transition metal atom in a linear M-C-O bond, the CO $5\sigma$ orbital donates electron density to a suitable metal $d_{z^2}$ orbital. This donation will create a negative charge on the metal atom, which is compensated via a back-donation from the metal $d_{xz}$ or $d_{yz}$ orbital to the unoccupied CO $2\pi^*$ orbital. As the CO $2\pi^*$ orbital is anti-bonding, populating it will result in a reduction in the bond strength of the CO molecule. This reduction can be seen as a reduction in the CO vibration frequency along the C-O axis,

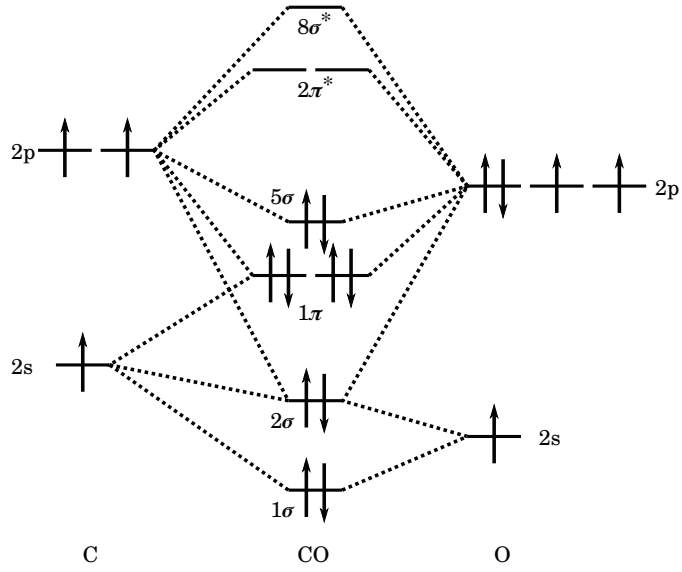


**Figure 3.1.** Molecular orbital diagram of CO.

which can be measured experimentally with infrared adsorption spectroscopy (IRAS). Thus, the shift in CO vibration frequency due to adsorption can be used as a tool to study the charge state of the surface.

## 3.3 Molecular dynamics

Molecular dynamics (MD) is a technique where one can follow the time evolution of a system of particles using the equations of motion, e.g. Newton's laws, together with an interaction potential between the particles. While the interactions can be calculated at the electronic-structure level [Car and Parrinello, 1985], one often uses simplified pairwise potentials in order to allow the simulation to proceed faster. For simulating large molecules such as biological systems or polymers, a common approach is to divide the interactions into two groups, bonded and non-bonded interactions. Bonded interactions refers to a short-range interaction between specific particles, thus simulating a covalent chemical bond. For instance, the bonds along a polymer chain would typically be modeled with bonded interactions. A typical and common bonded interaction term is a simple harmonic bond

$$U(r) = \frac{1}{2}k(r - r_o)^2,$$

where $r_0$ is the equilibrium bond length and $k$ is the spring constant. Other bonded interaction terms are e.g. angle potentials in order to simulate angle

dependent covalent bonds, torsion bonds to simulate higher bond orders, and so forth. The non-bonded interactions are then used to model the non-covalent bonding such as van der Waals (vdW) binding and electrostatic effects. The vdW effect is typically taken into account by the 12-6 Lennard-Jones bond

$$U(r) = 4\epsilon \left[ \left(\frac{\sigma}{r}\right)^{12} - \left(\frac{\sigma}{r}\right)^{6} \right], \tag{3.2}$$

where $\epsilon$ is the potential well depth and $\sigma$ specifies the range at which the potential $U(\sigma) = 0$. The energy minimum $-\epsilon$ is at $r = 2^{1/6}\sigma$. In the Lennard-Jones model the $r^{-6}$ term corresponds to the vdW interaction whereas the $r^{-12}$ term approximates the short-ranged covalent interaction. For a thorough introduction to MD, see e.g. Ref. [Leach, 2001].

### 3.3.1 Coarse-grained molecular dynamics

While an atomistic MD scheme with simple pair potentials is vastly faster than a full *ab initio* treatment, it is still too slow for many situations which requires the simulation of large systems over a long period of time. For instance, in an entangled polymer melt, the reptation theory [de Gennes, 1971] tells us that the equilibration time scales as $N^3$, where $N$ is the number of monomers in a polymer chain. Even for relatively short chains, this leads to very large relaxation times, which are far from feasible with an atomistic MD approach. One approach to solve this problem is the coarse-grained MD, where instead of simulating individual atoms one simulates *beads* consisting of several atoms. Due to the effectively smaller system, and the smoother potentials of the beads, a speedup of up to five orders of magnitude is not uncommon.

By coarse-graining one usually means an approach whereby one tries to map the atomistic system to the coarse-grained one in a systematic fashion. This is often done in an iterative manner, when the coarse-grained potentials are tuned to match the properties of the atomistic system. In the computational biophysics community, the popular MARTINI approach [Marrink et al., 2004, 2007, 2008, Monticelli et al., 2008] calibrates the coarse-graining potentials by using thermodynamic data, in particular matching the partitioning coefficients. Other approaches match e.g. gyration radius and inverting angular distributions to create angular potentials.

## 3.4 Multiscale modeling

Multiscale modeling [Nieminen, 2002] refers to using multiple simulation techniques in order to reach longer time and length scales, while keeping high ac-

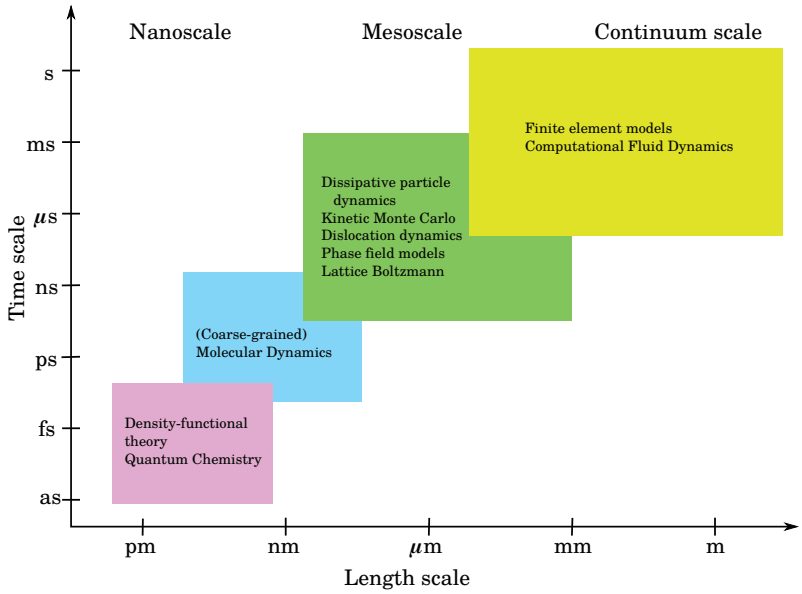


**Figure 3.2.** Example of simulation methods that can be used in a multiscale modeling approach.

curacy when and where needed. The canonical multiscale problem is brittle fracture [Broughton et al., 1999], where close to the crack tip one needs high accuracy, up to even the electronic structure level, but one still needs to simulate a very large system over a long time in order to study the crack dynamics. Due to the brittleness of the material, handling the boundaries between different scaling regions in the simulation system becomes crucial. Typically various approaches suffer from either reflection of high frequency phonons at the boundaries, or from energy loss at the boundaries. This is to some extent unavoidable, as the lower accuracy regions are unable to represent such high-frequency phonons, as these regions consist of much more massive elements with slower dynamics. A diagram showing different approaches that are suitable for different length scales can be seen in Fig. 3.2.

For the type of simulations done in this thesis, this is not a problem. Polymers are, by comparison to many crystalline materials, soft and they can thus easily adsorb some elastic energy at the region boundaries without affecting the system as a whole. Also, for the work in this thesis, it has not been necessary to concurrently simulate at multiple scales, but rather we mainly approach multiscale modeling by using more accurate methods, such as DFT, to *parametrize* interaction potentials for coarser scaled models.

### 3.4.1 Hybrid model of Senda

Kim and Senda [Kim and Senda, 2007] have introduced a hybrid MD-continuum model, where a MD region is coupled to an enclosing continuum. The coupling between the two regions can be seen as an extended version of the Andersen constant pressure MD method [Andersen, 1975], where the constant external pressure in the Andersen method is replaced by a varying pressure which is due to the continuum dynamics. The continuum dynamics is coupled to the MD model by adding the finite element (FE) contributions from the continuum to the Andersen Lagrangian. Conceptually, this is equivalent to connecting the MD system to a system of massive beads (the FE nodes) connected by springs (the FE stiffness matrix). This allows the simulation of a large system, where a small fraction can be treated with MD and larger scale phenomena with FE continuum mechanics.

An interesting use case for the hybrid MD-continuum model is to use the external system to drive the MD system towards equilibrium faster, as has been done in Publication IV. This is a big issue for polymer simulations, as the relaxation time for polymer melts with long chains are extremely long. The dynamics of polymer melt is in the reptation regime and, thus, relaxation time scales as $N^3$, where $N$ is the number of monomers. In the hybrid model, the fluctuating external pressure makes it easier for the entangled polymer melt to overcome potential barriers and, hence, it more quickly samples the available phase space and, thus, relaxation towards the equilibrium is also faster.

# 4. Simulating the polymer-metal interface

In order to thoroughly understand the interface between a metal and a polymer, there are multiple adhesion mechanisms that need to be understood, such as mechanical gripping, and multiple phenomena affecting the strength of the interface, such as the surface roughness and wetting. In engineering applications, the different heat expansion coefficients of the metal and polymer can cause large strain that weakens the interface [Luukkonen et al., 2011]. However, in this work we have focused on the interactions at the microscopic level. We use various model systems to study various aspects of the interactions, such as carbon monoxide (CO) to study the effect of transition metal doping of the surface and bisphenol-A-polycarbonate (BPA-PC) on an oxidized aluminium [Hoikkanen et al., 2008] surface to study the interaction of fragments of the BPA-PC polymer on the surface. In particular, BPA-PC on aluminium is an interesting combination for engineering applications, as both alumina and various polycarbonates are widely used, have beneficial properties, and are cheap. In practical applications exposing aluminium to the atmosphere causes the aluminium surface to oxidize such that an alumina layer is formed on the surface. Thus, we have mainly studied the interaction of BPA-PC with an alumina surface. To investigate the effect of the oxygen coverage, we have also studied how the oxygen coverage affects adsorption.

The adhesion of bisphenol-A-polycarbonate (BPA-PC) on aluminium depends strongly on the adsorption energetics of the phenyl end group of the polymer adsorbing on the aluminium surface, due to steric blocking [Delle Site et al., 2002]. For a schematic of a BPA-PC monomer, see Fig. 4.1.

Accurate electronic-structure calculation of the polymer interaction for complete polymer chains are not feasible and, thus, one must limit the size of the system somehow. We have used a building block approach where the polymer chain is broken down into chemical units, *fragments*. In contrast to simulating entire polymer chains, simulating individual fragments on a surface with DFT

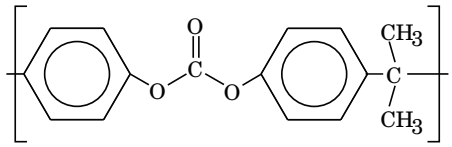

**Figure 4.1.** A BPA-PC monomer.

is a realistic proposition. However, the building-block approach may distort the simulation results compared to a simulation of an entire polymer chain. For instance, how does one replace the bonds between the fragments? A common approach is to passivate the dangling bonds by putting hydrogen atoms in place of the next fragment in the polymer chain. There are two potential problems with this approach. One is the question to which extent the replacement of the neighboring fragment with a hydrogen atom changes the electronic structure of the fragment, which may influence the covalent interaction with the substrate. The second issue is the steric effect of the neighboring fragments of the polymer chain, that is, how the rest of the polymer chain restricts the conformation of the fragment under study. We have tackled these issues by including the nearest-neighbor fragments in the simulation system. This moves the effect of the hydrogen passivation to the neighbor fragments and, thus, reduces their effect on the fragment closest to the surface. The neighboring fragments also provide some amount of steric constraints for the fragment closest to the surface, as the strong angle-dependent covalent bonds between the fragments will limit the conformations of the fragment closest to the surface.

## 4.1 Density-functional theory calculations

### 4.1.1 Effect of transition metals on the adsorption on oxide surfaces

The adsorption of particles on surfaces can greatly be affected by the presence of various kinds of impurities on the surface. This is widely used e.g. in heterogeneous catalysis, where catalyst particles are deposited on a support surface. As a model system for studying these issues, we studied the adsorption of carbon monoxide (CO) on a few low-index oxide surfaces both with and without the presence of small amounts of transition metal impurities. The surfaces chosen were MgO(001), $TiO_2$(110), and $Al_2O_3$(0001), as these surfaces have been extensively studied, and the surface orientations are those which give the lowest surface energy for the respective materials [Ramamoorthy et al., 1994, Spoto et al.,

2004, Godin and Lafemina, 1994]. These surfaces are also widely used in industrial applications, e.g., $TiO_2$ is widely used due to its photocatalytic properties in a wide variety of applications ranging from self-cleaning surfaces, paints, and sunscreens [Agrios and Pichat, 2005] to optically activated nanomedicine for treating cancer [Rozhkova et al., 2009]. MgO and $Al_2O_3$ have also been widely used, e.g., as catalyst support materials.

In heterogeneous catalysis, a porous support material such as alumina provides a very large surface area for the actual catalyst particles [Somorjai, 1994]. These catalyst particles are carefully chosen depending on which chemical reaction one wants to catalyse. Typically it turns out that transition metals such as Fe, Ag, Cu, Pd, and Pt, have the desirable properties. However, also the size of the catalyst particles have an effect and, thus, by changing the size of the particles one can also tune the catalytic properties [Xu et al., 1994, Bell, 2003, Lei et al., 2010]. An additional goal with changing the size of the catalyst particles is that the catalyst materials are often relatively expensive and, thus, smaller particles, with a larger surface to volume ratio, could provide the required reaction rate with less consumption of the expensive materials.

In Publication I we studied what effect the presence of atomic Ag or Pd had on the adsorption of CO on the chosen oxide surfaces. In order to enable comparisons with IRAS experiments and calculations, we calculated the change in the major mode vibrational frequency of the CO molecule as a result of the adsorption onto the surface. As the change in vibrational frequency of the molecule can be used experimentally as a probe into the charge state of the adsorption site, as explained in Section 3.2.3, we have also studied the Bader charges on the CO molecule and, in the case of adsorption on top of the transition metal adatoms, the Bader charge on the adatom as well. We found that, in general, the adsorption is enhanced by the presence of the transition metal adatoms, in particular the Pd did strongly increase the adsorption. In all the cases, the CO molecule preferred to adsorb on top of the adatom, although in a few cases in a tilted position rather than upright. A summary of the findings can be found in Table 4.1.

The relationship between the change in the CO vibration frequency and the Bader charge on the transition metal adatom can be seen in Fig. 4.2. This shows that the relationship is roughly linear, as predicted e.g. in Ref. [Márquez et al., 2010]. In general, our results suggest that small amounts of appropriate transition metals can greatly affect the adsorption of organic molecules. This could be used in pre-treating metal surfaces before the introduction of a polymer melt on the surface, thus allowing the properties of the polymer-metal

**Table 4.1.** Summary of the largest CO adsorption energies on the studied surfaces. In all cases the CO molecule prefers to adsorb with the C atom closer to the surface. In the $q_{Ag/Pd}$ rows one can see the Bader charge on the transition metal adatom before and after the adsorption of the CO molecule, whereas the $q_{CO}$ rows show the Bader charge on the CO molecule after the adsorption. The $\Delta\nu$ rows show the shift in the vibration frequency of the CO molecule compared to the vacuum. For details see Publication I.

| | | MgO | $TiO_2$ | $Al_2O_3$ |
|---|---|---|---|---|
| Clean | $E_{ads}$(eV) | 0.16 | 0.32 | 0.51 |
| | $q_{CO}(e)$ | −0.06 | 0.03 | −0.01 |
| | $\Delta\nu$ ($cm^{-1}$) | −7.9 | 38.4 | 38.6 |
| | Site | Mg | Ti(5f) | various |
| Ag | $E_{ads}$(eV) | 0.45 | 1.31 | 0.61 |
| | $q_{Ag}(e)$ | −0.09/0.09 | 0.54/0.67 | 0.36/0.55 |
| | $q_{CO}(e)$ | −0.19 | −0.03 | −0.12 |
| | $\Delta\nu$ ($cm^{-1}$) | −232.1 | −24.1 | −69.2 |
| | Site | Ag top tilt | O(p) | Ag top |
| Pd | $E_{ads}$(eV) | 2.54 | 2.01 | 2.38 |
| | $q_{Pd}(e)$ | −0.21/−0.07 | 0.35/0.39 | 0.18/0.16 |
| | $q_{CO}(e)$ | −0.12 | −0.11 | −0.10 |
| | $\Delta\nu$ ($cm^{-1}$) | −83.9 | −78.4 | −67.5 |
| | Site | Pd top | Pd top | Pd top tilt |

interface to be tuned according to the needs of the application.

### 4.1.2 Adsorption of BPA-PC fragments on clean and oxidized aluminium surfaces

We have used DFT to study the interaction of BPA-PC fragments with aluminium and alumina surfaces in Publications II and III. For the individual fragments, we studied benzene ($C_6H_6$), carbonic acid ($H_2CO_3$), and isopropylidene ($C_3H_8$), where the dangling bonds were passivated with hydrogen atoms. Also, we studied phenol ($C_2H_5OH$), as some previous studies suggested that phenol binds to the alumina surface via the OH group [Chakarova-Käck et al., 2006], and the benzene-carbonic acid bond in the BPA-PC monomer can perhaps better be described by using a phenol fragment rather than a benzene fragment. In general, for the single fragments on the clean and oxidized Al(111) surface we found that the adsorption was nonexistent, with the exception of benzene on an oxidized Al(111) surface with 0.125 ML oxygen coverage, where the adsorption energy for the most favorable site was 0.52 eV. The different adsorption sites on the alumina surface can be seen in Figure 4.3.

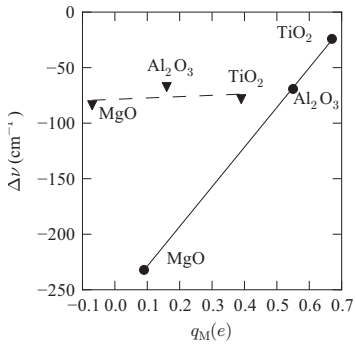


**Figure 4.2.** Shift in the CO vibration frequency as a function of the Bader charge on the Ag (circles) and Pd (triangles) adatoms. The lines are the least-squares fittings to the data.

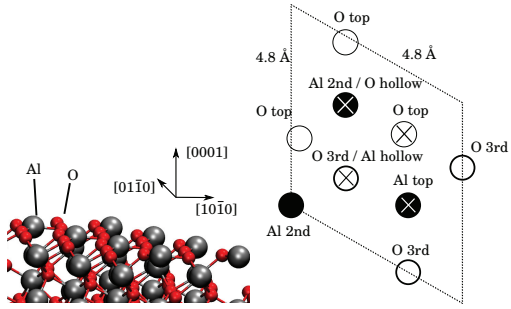


**Figure 4.3.** General view (left) and surface atoms (right) on the Al-terminated $\alpha$-$Al_2O_3$(0001) surface. On the left, Al atoms are larger gray spheres and O atoms smaller red spheres (dark gray spheres in b/w). On the right, Al atoms are filled circles and O atoms empty circles. Due to the $Al_2O_3$ surface relaxation, the uppermost Al and O layers are almost at the same height, then the second layer with Al atoms, and finally the third layer with O atoms. A 2×2 surface supercell box can also be seen.

For the alumina surface, benzene preferably adsorbed weakly on the O top site on the surface, with an adsorption energy of only 0.1 eV. As expected we found that the phenol molecule did adsorb more strongly than benzene, with an adsorption energy of 0.66 eV, interacting mostly via the OH group as previous studies suggested [Chakarova-Käck et al., 2006]. Similar to the Al(111) surface, the propane molecule did not adsorb at all on the alumina surface. The carbonic acid molecule, however, adsorbed strongly on the alumina surface. During the adsorption, one of the passivating hydrogens detached from the molecule and adsorbed at the surface O-top site. This configuration, with a reduction in total energy of −1.91 eV, can be seen in Fig. 4.4. Separating the contributions from the carbonic acid molecule and the hydrogen atom revealed that much of this energy was due to the rearrangement of the bonding of the hydrogen atom. The bond dissociation energy for the hydrogen atom from the carbonic acid molecule in vacuum was found to be −5.74 eV, whereas the adsorption of a hydrogen atom at the O-top site on the $\alpha$-$Al_2O_3$(0001) surface was −4.14 eV. Hence there was a change in the binding energy of the hydrogen atom of +1.60 eV when it switched from the carbonic acid molecule to the surface and, thus, in the above system the contribution of the carbonic acid molecule to the total adsorption energy of −1.91 eV was −3.51 eV. Experimental results show qualitatively similar behavior [Su and Suarez, 1997, Alliot et al., 2005]. Thus, while the dissociation of one of the passivating hydrogen atoms from the carbonic acid molecule is an interesting phenomena per se, it is not desirable if the goal is to study interaction of polymer chains with the surface. Of course, it is also possible that the interaction with the surface could cause the polymer chain to break up, similar to how the passivated carbonic acid molecule broke up, but this would require further in-depth study of the break-up mechanism including the nearest-neighbor fragment instead of the passivating hydrogen.

### 4.1.3 Role of the van der Waals interaction and nearest-neighbor fragments

In Publication III we have extended a subset of the calculations in Publication II by incorporating two effects, namely the van der Waals (vdW) interaction and nearest-neighbor fragments instead of hydrogen passivated dangling bonds. The molecules with closed shells interact very weakly via the covalent interactions modeled by traditional DFT, whereas the vdW interaction is, technically, a double integral over the electron density and, thus, is not directly affected by orbitals being closed or not. Hence, one can expect that large closed shell molecules interact mostly via the vdW interaction and correspondingly that the

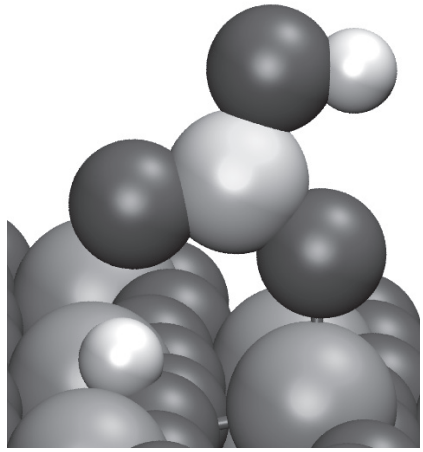

**Figure 4.4.** A carbonic acid molecule adsorbed on the $\alpha$-$Al_2O_3$(0001) surface. Hydrogen atoms are seen as small light gray spheres, carbon as large light gray spheres, oxygen as large black spheres, and aluminium as large dark gray spheres.

covalent interaction would be relatively weak. Similarly, including the nearest-neighbor fragments instead of passivating dangling bonds with hydrogen atoms provides a more realistic environment for the fragment under study, as well as providing steric constraints. The dangling bonds of the nearest-neighbor fragments, in turn, are passivated by hydrogen atoms, however, their effect on the fragment under study should be smaller than without the nearest neighbors.

The nearest-neighbor fragments introduce some new challenges for the simulations. They increase the size of the system and they increase the space over which one needs to search for the energy minimum. Relaxing the system with an accurate DFT-GGA calculation is too time-consuming, so instead we have first relaxed the systems with a quick LCAO DFT-GGA method and then switched to the more accurate method, once the LCAO relaxations are complete. Furthermore, with the LCAO method we can quickly scan many different starting positions for the systems and for the more accurate calculations we have continued only with the most promising conformations for each system. The LCAO calculations have been done with the Siesta simulation program [Soler et al., 2002], whereas for the more accurate calculations including the vdW interactions we have used the finite difference DFT package GPAW [Mortensen et al., 2005, Enkovaara et al., 2010]. Siesta uses numerical atom-centered basis functions, whereas GPAW uses a finite-difference scheme on a regular grid. In order to avoid the problem of needing a very dense grid due to the rapidly varying wavefunctions close to the atomic cores, GPAW uses the projector augmented wave (PAW) scheme [Blöchl, 1994]. Both simulation packages were controlled via the Atomic Simulation Environment (ASE) [Bahn and

Jacobsen, 2002], which was also used to construct the supercells used in the simulation.

In GPAW, the vdW interactions are taken into account by using the FFT-based method by Román-Pérez and Soler [Román-Pérez and Soler, 2009]. The GGA functionals used in the simulations were the revised version [Hammer et al., 1999] of the PBE [Perdew et al., 1996, 1997] functional for the LCAO calculations, and for the vdW-DFT calculations the covalent exchange part was simulated using another revised version (revPBE) of the PBE functional [Zhang and Yang, 1998]. In order to speed up the LCAO calculations single-$\zeta$ polarized (SZP) orbitals were used, meaning that there was only a single basis function for each valence state in the system, and an additional basis function corresponding to the lowest unoccupied angular-momentum quantum number. Also, only a single k-point was used. On the other hand, for the finite-difference calculations, a grid spacing of 0.19 Å was used, and a denser k-point grid consisting of a 2x2x1 Monkhorst-Pack mesh [Monkhorst and Pack, 1976, Pack and Monkhorst, 1977]. For the LCAO calculations, the inter-atomic forces were relaxed until they all were smaller than 0.04 eV/Å, whereas for the FD vdW-DFT calculations 0.02 eV/Å was used as the stopping criterion.

Due to the large size of the polymer fragment molecules compared to the previous work in Section 4.1.2, the simulation cells were much larger in this case. Our slab contained 96 Al and 144 O atoms in 12 Al and 6 O layers, forming an 8x4 hexagonal surface supercell. For some of the LCAO calculations, depending on the rotational configuration of the polymer fragments, the slab size was further doubled to a 8x8 surface supercell.

The fragments of a BPA-PC monomer, see Figure 4.1, are phenol (P, chemical formula $C_6H_4$), carbonic acid (C, $CO_3$), another phenol fragment, and isopropylidene (I, $C_3H_6$). We thus studied various combinations of these building block fragments along with their nearest neighbors. Since the BPA-PC polymer chain is always terminated by a phenol fragment, for the chain ends we studied a PC segment. The other possible termination, that is the PI segment, was not studied because the I fragment prevents the P fragment from getting close to the surface. For the segments inside the polymer chain, we studied the PCP, IPC, and IPC segments. For the dangling bonds we substituted hydrogen atoms. The initial configurations of segments on the surface was chosen such that various adsorption sites on the alumina surface were matched with the atom in the segment which was placed closest to the surface. The adsorption sites on the alumina surface can be seen in Figure 4.3. For each adsorption location, the segment was rotated at 30° intervals. This was repeated for all the stud-

**Table 4.2.** Calculated adsorption energies of the BPA-PC segments with the vdW-DFT method. In the first column, the total vdW-DFT energy is shown, the second column contains the GGA contribution (that is, the energy without the vdW interaction), and the third column is the vdW energy.

| | $E_{ads}$(eV) | $E_{ads,revPBE}$(eV) | $E_{ads,vdW}$(eV) |
|---|---|---|---|
| PC | 1.22 | 0.42 | 0.80 |
| PCP | 1.49 | 0.22 | 1.26 |
| IPC | 1.47 | 0.32 | 1.15 |
| PIP | 0.90 | 0.03 | 0.88 |

ied segments, leading to a total of 240 different configurations, some of which were equivalent due to rotational symmetry. The symmetrically non-equivalent configurations were then relaxed with the LCAO method, after which for each segment the most favorable configuration was selected for relaxing further with the finite-difference vdW-DFT method. Generally, there was little difference between the different adsorption sites, which can be understood when one considers that the polymer segments studied are large and interact with the surface over a wide area, particularly for the vdW-DFT calculations where the vdW interaction is considerably longer ranged than the covalent interaction range.

The results for the adsorption of the segments with the vdW-DFT method can be seen in Table 4.2. For all the cases one can clearly see that the vdW contribution is a significant, if not the dominant, factor in the total adsorption energy. In particular, for the PIP case there is practically no GGA interaction at all. This can be understood also by looking at the adsorption geometries in Figure 4.5, where one can see that the PIP segment is positioned quite far from the surface. One reason for this is that the hydrogen atoms on the isopropylidene fragment are pointed downwards towards the surface, preventing the rest of the atoms from getting closer.

## 4.2 Surface interaction potentials

Using the results from our adsorption energy calculations in Section 4.1.3, we can parametrize surface interaction potentials for the use in coarse-grained molecular-dynamics calculations. However, the presence of the nearest-neighbor fragments means that the adsorption energies of the individual fragments are not directly available. One approach to solve this is to calculate the individual fragments in a fixed geometry as calculated in the multi-fragment calculations with the neighboring fragments included, again passivating the dan-

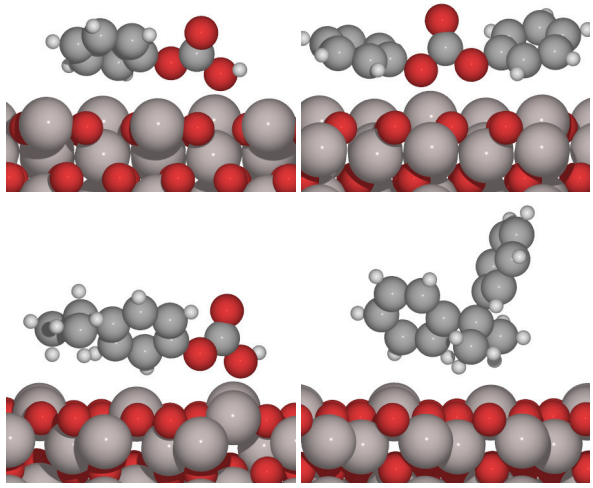

**Figure 4.5.** Adsorption geometries for the BPA-PC segments on the alumina surface. The segments are PC (top left), PCP (top right), IPC (bottom left), and PIP (bottom right). Red spheres (dark gray spheres in b/w) represent O atoms, large gray spheres Al atoms, gray spheres C atoms, and small gray spheres represent H atoms.

gling bonds with hydrogen atoms. However, in our experience this did not work very well, as rebuilding the multi-fragment segments using the fitted single-fragment potentials resulted in large energy differences up to 0.7 eV compared to the multi-fragment vdW-DFT calculation results. Thus, we instead fitted the potentials for the individual fragments directly from the multi-fragment DFT data. To generate data for the adsorption energy as a function of the distance from the surface, we made further calculations by changing the height of the segments from the surface, however, no geometry optimization was done in this case. This data can then be fitted to a suitable function. For the fitting procedure we fitted the sums of the individual fragments to the calculated multi-fragment DFT results. A number of different functions were tested. Often, in molecular-dynamics simulations one uses Lennard-Jones style potentials in order to simulate long-range van der Waals interactions. Thus, we used a number of different Lennard-Jones style potential functions for testing. The basic Lennard-Jones potential is the so-called 12-6 potential, which can be seen in Equation (3.2). This potential models the interaction between two point particles. However, in this case we are interested in modeling the interaction of a molecule with a surface slab. We approximated each fragment as a point particle, as this approximation was also used in the coarse-grained bulk polymer model. The different potential functions tested differed in how the surface was treated. If one integrates the 12-6 LJ potential between a point particle and a

semi-infinite slab of uniform density one gets a 9-3 LJ potential

$$U(r) = 3\sqrt{\frac{2}{5}}\epsilon\left[\frac{1}{15}\left(\frac{\sigma}{r}\right)^9 - \frac{1}{2}\left(\frac{\sigma}{r}\right)^3\right].$$

However, if one assumes that only the surface layer of the slab interact with the particle, with the lower lying layers screened by the surface, one gets a 10-4 LJ potential

$$U(r) = \frac{5}{3}\epsilon\left[\frac{2}{5}\left(\frac{\sigma}{r}\right)^{10} - \left(\frac{\sigma}{r}\right)^4\right].$$

Finally, we also tested a Steele 10-4-3 LJ potential [Steele, 1973] of the form

$$U(r) = 2\pi\rho_S\Delta\sigma^2\epsilon\left[\frac{2}{5}\left(\frac{\sigma}{r}\right)^{10} - \left(\frac{\sigma}{r}\right)^4 - \frac{\sigma^4}{3\Delta(r+\alpha\Delta)^3}\right],$$

where $\Delta$ is the spacing between basal planes in the surface and $\alpha$ is a free parameter. The 10-4-3 potential models a single surface layer at distance $r$ followed by a semi-infinite slab at a distance of $\alpha\Delta$ from the first layer.

In the fitting procedure we fitted sums of single-fragment LJ potentials using the calculated multi-fragment DFT results as the reference. The distance from the surface of each of the single fragments, which were modeled as point masses, was taken as the distance of that fragment in the multi-fragment DFT simulations. We simultaneously fitted the sums P+C, P+C+P, I+P+C, and P+I+P and minimized the difference to the DFT results in the least-squares sense. The parameters for the fitting procedure were the $\sigma$ and $\epsilon$, and in the case of the 10-4-3 potential additionally $\alpha$, for each fragment type. Of the various LJ potentials, the 10-4-3 potential was the best choice, in terms of having the smallest residual. However, the 10-4 potential was only marginally worse, and thus the inclusion of an extra parameter for the 10-4-3 potential ($\alpha$) was not justifiable. The fitted 10-4 potentials compared with the multi-fragment vdW-DFT results can be seen in Figure 4.6. While the fits are not perfect, they are quite good considering that the fragments have been approximated as point masses, the surface is approximated as a simple featureless wall, the 10-4 LJ potential is a simple function with only two free parameters, as well as inaccuracy due to the building block approach where we approximate the multi-fragment segments as a simple sum of single-fragment potentials. In particular, the PCP and IPC fits are quite good, and those are the most important considering that PC is only at the chain ends and, thus, does not have as much opportunity to contribute to the total adsorption of a polymer chain as the other three segments, and that the PIP interaction is weak by comparison.

In Table 4.3 one can see the fitted potential parameters $\epsilon$ and $\sigma$, as well as single fragment averaged vdW-DFT adsorption energies at the equilibrium distance for comparison. The averaging has been done by calculating the individ-

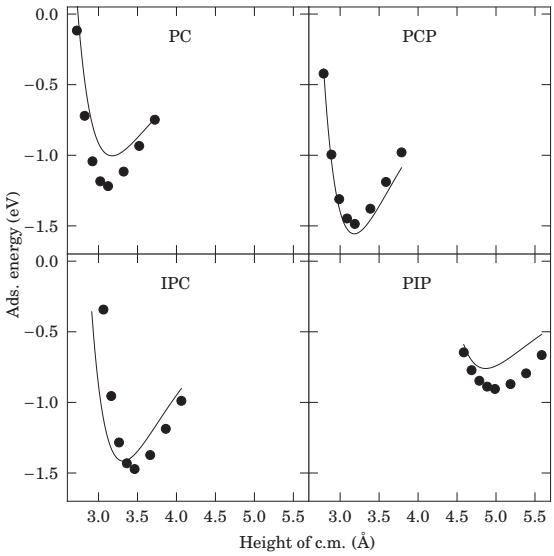


**Figure 4.6.** Adsorption energies of the multi-fragment segments calculated using vdW-DFT (circles), compared to the corresponding sums of the fitted 10-4 Lennard-Jones potentials (solid lines).

**Table 4.3.** Fitted 10-4 Lennard-Jones potential parameters for the fragments. vdW-DFT adsorption energies and equilibrium distances between the surface and the fragment center-of-mass for single fragments are included for comparison in the two rightmost columns.

| | $\epsilon$ (eV) | $\sigma$ (Å) | $E_{\text{ads}}$(eV) | $z$ (Å) |
|---|---|---|---|---|
| P | 0.50 | 3.02 | 0.30 | 3.54 |
| C | 0.57 | 3.12 | 0.59 | 3.05 |
| I | 0.50 | 3.43 | 0.18 | 3.59 |

ual fragments in the geometries as calculated by the multi-fragment calculations, that is, for the PC segment both P and C, for the PCP segment C, for IPC P, and finally for the PIP segment I was calculated. Then the results for the C and P beads which occur twice have been averaged. Due to the choice of pre-factors in the 10-4 LJ potential, the minimum energy for that potential is at the distance $\sigma$ from the surface and, thus, $E_{\text{min}}(\sigma) = -\epsilon$. Thus, the fitted parameters can be directly compared to the results from the DFT calculation of the individual fragments. The strongest adsorption in both the fitted and calculated cases is for the C fragment, however, for the I fragment the fitted adsorption energy is much higher than the calculated. This can be understood by considering that the PIP segment has a different conformation on the surface compared to the other segments, with the P fragments located far from the surface, which the fitting procedure only indirectly takes into account.

| | C | P | I |
|---|---|---|---|
| $\sigma$ (nm) | 0.349 | 0.467 | 0.519 |

**Table 4.4.** Sizes of the beads in the coarse-grained BPA-PC model. The beads are carbonic acid (C), phenylene (P), and isopropylidene (I). The masses of the beads are 73 u, which is the average of the bead masses.

## 4.3 Coarse-grained molecular dynamics of polycarbonate

### 4.3.1 System

For simulating coarse-grained polycarbonate, we have used an existing model for the bulk and focused on developing potentials for the metal-polycarbonate interface based on the model presented in Publication III. The bulk model for coarse-grained polycarbonate has been described in more detail in Refs. [Abrams et al., 2003, Delle Site et al., 2002, 2003]. The BPA-PC monomer, see Fig. 4.1, is modeled as 4 beads, where the beads represent the phenylene ring, the carbonic acid, and the isopropylidene. The sizes of the beads can be seen in Tab. 4.4. In contrast to previous work using the same BPA-PC model for the bulk, we did not use reduced Lennard-Jones units. Also, the harmonic bonds between the beads were replaced with constraints, where the constraint system was solved with the parallel linear constraint solver algorithm P-LINCS [Hess, 2008]. This allowed longer timesteps without significantly affecting the physics of the model, which was mostly contained in the non-bonded interactions and the angle potentials. We simulated the canonical ensemble with the temperature kept at 570 K using a Langevin thermostat with a friction coefficient of 0.29ps$^{-1}$, corresponding to a friction coefficient of 0.5$\tau^{-1}$ in reduced units. For the simulations we used the GROMACS package [Lindahl et al., 2001, Hess et al., 2008, Berendsen et al., 1995, Van Der Spoel et al., 2005]. The bead density of the bulk system was 9.91 nm$^{-3}$, corresponding to the typical experimental melt density of 1.05 g cm$^{-3}$. However, due to the chain terminations the actual bead density in the simulations were slightly different.

The surface interaction was modeled by parametrizing 10-4 Lennard-Jones interactions using our results in Publication III. In contrast to previous studies of BPA-PC on Ni(111) [Delle Site et al., 2002], we found that the carbonic acid bead exhibited the strongest adsorption. Hence our results were qualitatively different from the Ni(111) case, since on the Ni(111) surface it was found that only the phenyl endgroup adsorbs to the surface.

For the bulk calculations we used two systems of different size, and for the

**Table 4.5.** Studied polymer systems. $N$ is the number of monomers in a polymer chain, and $4N+3$ is the number of beads in each chain. The third column, $n$, is the number of chains in the system. In the fourth column one can see the dimensions of the simulation box. $R_g$ is the radius of gyration, and $R_{e-e}$ is the mean end-to-end distance of the polymer chains in the system.

| $N$ | $4N+3$ | $n$ | box dim (nm) | type | $R_g$(nm) | $R_{e-e}$(nm) |
|---|---|---|---|---|---|---|
| 10 | 43 | 80 | 7x7x7 | bulk | 2.046 | 5.581 |
| 10 | 43 | 80 | 7x7x7.5 | surf | 1.767 | 4.364 |
| 20 | 83 | 100 | 9.43x9.43x9.43 | bulk | 2.598 | 6.510 |
| 20 | 83 | 100 | 9.43x9.43x9.93 | surf | 2.521 | 6.182 |

surface calculations we used equivalent systems where the polymer lengths were the same as in the bulk systems.

### 4.3.2 Results

We equilibrated the system by starting from a random walk generated such that the bead distances and average angles are correct. After this we did a short potential-energy minimization run with 200 steps and capped non-bonded forces and potentials in order to reduce the overlap of the beads. Capping the forces at some maximum value in this initial stage was necessary in order to smoothly allow overlapping particles to move away from each other. Following this we did the actual molecular-dynamics relaxations while slowly increasing the maximum force and potential until the capping could be completely removed. The relaxation of the system was monitored via the mean-square internal distance measure [Auhl et al., 2003], as well as the radius of gyration. The mean-square internal distance $< R^2(n) >$ is defined as the average distance between all beads which are separated by $n$ beads in the polymer chains. The equilibrium properties of the system can be seen in Tab. 4.5. They match previously published results using similar BPA-PC models [Abrams and Kremer, 2003, Hess et al., 2006].

Compared to a system not using constraints, that is, where there are instead harmonic bonds between the beads in the chains, there is no change in the monitored quantities. However, without the constraints the stiff harmonic bonds forced a much smaller timestep, 0.0002 ps instead of 0.0015 ps used with the constrained system. Even though a large part of the simulation time is spent solving the constraint system, this constitutes a substantial speedup of the simulation.

In Fig. 4.7 one can see the mean-square internal distances of the larger bulk system during the relaxation. After roughly $10^8$ steps the system can be con-

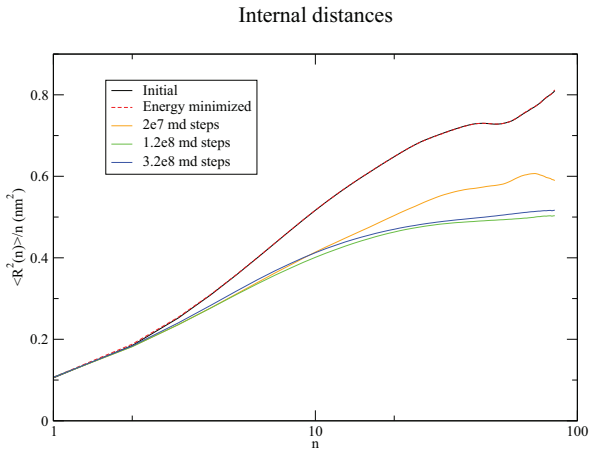


**Figure 4.7.** Internal distances of the bulk system with 100 chains of 83 beads each.

sidered equilibrated.

As the dynamics in the coarse-grained system are much faster than in an atomistic simulation, which in fact is one of the major reasons for the speedup of the simulations, the time in the coarse-grained model is not comparable to real time, as in an atomistic calculation. A common approach to map the coarse-grained time scale to the real time is by comparing diffusion coefficients. From Ref. [Hess et al., 2006] we find that the all-atom diffusion constant, that matches the experimentally observed value, is about $2.03 * 10^{-10}\mathrm{cm}^2\mathrm{s}^{-1}$. In our simulations of the 83 bead system, we find a diffusion constant of $3.84 * 10^{-7}\mathrm{cm}^2\mathrm{s}^{-1}$, hence find that the time scaling for our setup is

$$1 : 1900\,.$$

Our effective timestep is thus $\Delta t \approx 2.85$ ps.

For the systems with walls, the density profile shows the average chain components at the surface. For the smaller surface system with 43 bead polymers, this density profile can be seen in Fig. 4.8. One can see that within approximately 1.5 nm from the wall, the densities of the beads form layers. This effect becomes stronger the closer to the wall one gets and correspondingly vanishes in the bulk. This is due to the beads closest to the surface packing at a certain distance from the walls due to the attractive potential well. A few layers away from the wall this effect is still seen, but towards the bulk the random thermal motions of the beads destroy the layering. While the C bead has the strongest adsorption energy, the most common bead in the layer closest to the walls is P.

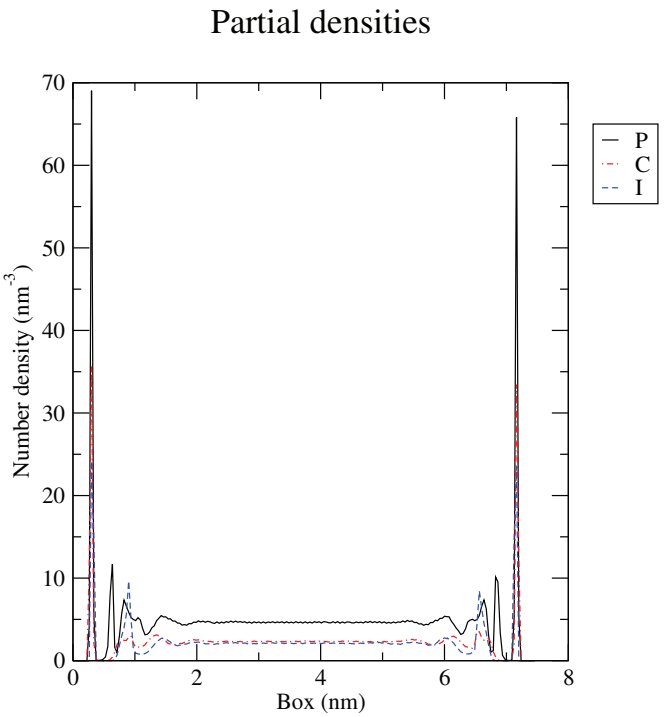


**Figure 4.8.** Density profile for the wall system with 80 polymer chains with 43 beads each. The number densities in the layer closest to the surface are approximately 67 (P), 34 (C), and 24 (I) nm$^{-3}$.

There are two reasons for this. First, the P beads are more common than the other types. A BPA-PC monomer contains two P beads, one C bead, and one I bead. This can also be seen in the bulk densities. Secondly, the chains are terminated by P beads and, thus, the P beads at the ends of the chains have better opportunity to come in contact via the surface, as the polymer melt chain dynamics is dominated by reptation. While the C and I beads are equally common, one can see that the C beads are more common close to the surface, which can be explained by the higher adsorption energy of the C beads compared to the I beads, as can be seen in Publication III.

In Figure 4.9 one can see a histogram which depicts the number of beads in each chain that are in contact with the surface for the surface system with 43 beads per chain and 80 chains in a 7x7x7.5 nm box. A bead is considered to be on the surface if it is within 0.5 nm of the box edges in the $z$ direction. As can be seen in Figure 4.8, 0.5 nm from the edges matches the first minimum in the density profile and, thus, the chosen criterion includes the first layer on the surface while more or less completely excluding other beads not in that first layer. One can see that slightly over half of the chains are not at all in contact with the surface, whereas for the rest the number of the beads that lie on the

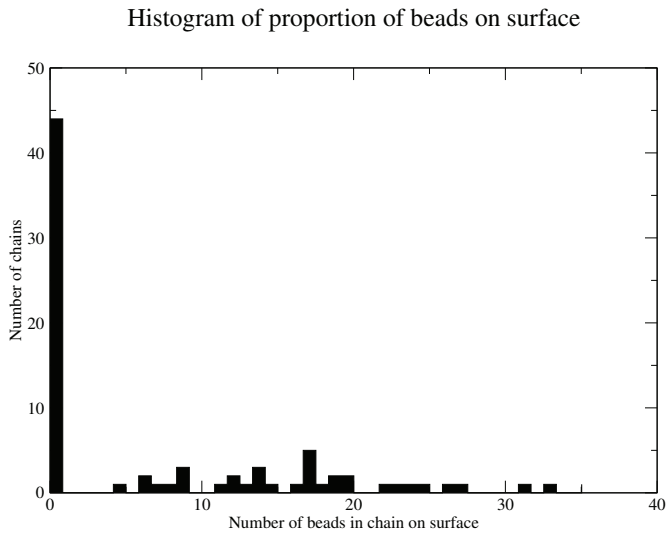


**Figure 4.9.** Histogram of the number of chains that are in contact with the surface. The system consists of 80 chains of 43 beads each, in a 7x7x7.5 nm box.

surface has a wide distribution between roughly 5 and 35 beads. One can also see that there are no chains with only one or two beads in contact with the surface.

From the density profile in Fig. 4.8 as well as the histogram in Fig. 4.9, one can see that there is no particular preference for adsorbing only via the chain ends, as was found to be the case e.g. for BPA-PC on a Ni(111) surface [Delle Site et al., 2002]. That is, the difference in electronic-structure interaction between the polymer beads and different surfaces drastically affects the configuration of the polymer chains close to the surface. An interesting topic for further study would be to characterize how this difference affects the strength of the interface. For BPA-PC on the Ni(111) surface, due to only the chain ends adsorbing to the surface, one can expect a hairbrush-style interface where on the surface one finds tightly packed chains with the chain ends contacting the surface. For the system studied here with BPA-PC on the $\alpha$-$Al_2O_3$(0001) surface, one can instead expect fewer chains in contact with the surface, but those chains to be much more strongly bonded as many beads along the chain length are in contact with the surface. Whether this will ultimately make the polymer-metal interface stronger could be studied e.g. with pulling simulations, where the polymer mass is pulled away from the surface.

## 4.4 Equilibration of polymer melts using the hybrid method

In Publication IV we have studied the usage of the hybrid model presented in Section 3.4.1 to equilibrate polymer melts. The model system used in this study is a bead-spring system, where the non-bonded interaction representing the excluded volume around each bead is described by a shifted and truncated 12-6 Lennard-Jones potential

$$U_{LJ}(r) = \begin{cases} 4\epsilon\left[\left(\frac{\sigma}{r}\right)^{12} - \left(\frac{\sigma}{r}\right)^{6} + \frac{1}{4}\right] & r \le r_c \\ 0 & r > r_c \end{cases},$$

with the cutoff radius $r_c = 2^{1/6}\sigma$. The bonded interaction between neighboring beads in the polymer chains is described by a finite extensible non-linear elastic (FENE) potential

$$U_{FENE}(r) = \begin{cases} -0.5kR_0^2 \ln\left(1 - \left(\frac{r}{R_0}\right)^2\right) & r \le R_0 \\ \infty & r > R_0 \end{cases},$$

where $k = 30\epsilon/\sigma^2$ and $R_0 = 1.5\sigma$. Additionally a harmonic bending potential

$$U_{bend}(\theta) = k_\theta(1 - \cos\theta),$$

where $\theta$ is the angle between neighboring beads and $k_\theta = 0.25\epsilon$, was used to add stiffness to the polymer chains. For the hybrid calculations, the polymer model above is connected with the elastic continuum as per Ref. [Kim and Senda, 2007]. The MD simulation cell is initially cubic, with a polymer bead number density of $0.85\sigma^{-3}$ and the initial temperature is set to $1.0\epsilon/k_B$. The simulations were performed with the ESPResSo package [Limbach et al., 2006].

The equilibration of the polymer system using the hybrid method was compared to that of equilibrating the system using the Andersen constant-pressure MD method. The change in the average end-to-end distance of the polymer chains during the equilibration showed that the hybrid method achieved equilibrium much faster than by using the Andersen constant-pressure MD. This can be seen in Figure 4.10. One can see that with the hybrid method there are large fluctuations in the average end-to-end distance. These fluctuations are due to the elastic continuum and allow the polymer melt system to overcome barriers in the potential energy landscape, thus leading to faster equilibration.

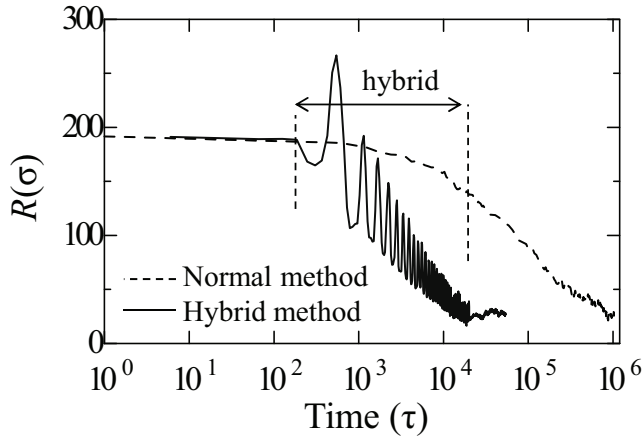


**Figure 4.10.** The end-to-end distances of the polymer melts as a function of simulation time. For the hybrid method one can see large fluctuations in the average end-to-end distance, which leads to faster equilibration.

# 5. Summary and conclusions

In this thesis I have studied some aspects of the interaction between polymers and metal surfaces, mostly at the microscopic electronic-structure level. Tuning the electronic structure is an essential part of heterogeneous catalysis (e.g. Ref. [Somorjai, 1994]), and there is every reason to believe it could also work for polymer adsorption as well. In Publication I the effect of a few transition metals on the adsorption of carbon monoxide on different oxide surfaces was studied. It was found that the presence of the transition metal atoms on the surface has a major effect on the CO adsorption, as well as on the charge transfer between the surface, the transition metal adatom, and the CO molecule. An interesting avenue for further research would be to study the effect of transition metal doping on a polymer-metal interface which could be studied experimentally as well. Transition metals should have an effect of increasing the binding beyond what only the vdW interactions can provide, thus allowing the engineering of stronger interfaces when that is desired by the application.

In addition to the effect of transition metal adatoms, the surface oxidation can also affect the surface electronic structure. As reported in Publication II, changes in the surface oxidization can have a major impact on the adsorption of the polymer chains at the surface. It is thus very important to have a clear and accurate understanding of the oxidation of the surface in order to achieve consistent adhesion. This was also experimentally studied, and summarized in Refs. [Hoikkanen et al., 2008, Luukkonen et al., 2011].

At the electronic structure level, the inclusion of the nearest neighbors and the van der Waals interactions can have a dramatic effect, as can be seen in Publication III. In a multi-scale simulation where the coarser-scaled models are parametrized from finer-grained calculations, errors in the fine-grained electronic-structure calculations cascade to the coarser-grained models as well. It is very important that these finer-grained calculations are done very carefully, including all the energetically relevant interactions.

Finally, when taking the multi-scale approach further one eventually wants to couple atomic and continuum mechanics systems. The hybrid approach by Senda et al. [Kim and Senda, 2007] offers one approach for this. As a side-effect of this coupling between the atomistic and continuum systems, in Publication IV we have used the hybrid model as a tool to achieve faster convergence towards the ground state when equilibrating polymer chains. The equilibration of long polymer chains is a substantial challenge for the simulation of polymer chains, as the relaxation time scales as $N^3$ as per the reptation theory of de Gennes [Rubinstein and Colby, 2003], and a naive relaxation approach for a melt of realistically long chains is beyond the capability of even the fastest computers. In the hybrid model, the acceleration of the relaxation is achieved by the elastic continuum producing large volume and pressure fluctuations in the atomistic region, which helps the molecular dynamics simulation of the polymer dynamics to overcome energy barriers, thus leading to faster relaxation towards the ground state.

As this thesis has focused on various microscopic scale phenomena, there are still many interesting topics to explore before one can achieve the goal of a fully hierarchical multi-scale model, such as presented e.g. in Fig. 3.2, describing the polymer-metal interface. Such a model would provide a link between the quantum-mechanical models that have been the focus of this thesis and the engineering issues that applications of these hybrid materials face. Thus, it would be possible to study systematically e.g. how a change in the microscopic surface interaction due to the addition of small amounts of transition metals on the surface would affect the macroscopic properties. Also, in the case of nanocomposite materials such as layered structures consisting of very thin layers, mesoscale models in between the microscopic models studied in this thesis and the continuum models used in the macro-scale, could provide a valuable tool for predicting the properties of such exotic composite materials.

In general, multi-scale modeling is an extremely attractive tool to understand complex materials, however, significant work is still needed for each material in question. Ultimately, a hierarchical multi-scale approach asks the scientist to identify the relevant factors at each scale which affects the next-scale model and, thus, linking the different scale models together.

# Bibliography


C. F. Abrams and K. Kremer. Combined coarse-grained and atomistic simulation of liquid bisphenol-a-polycarbonate: Liquid packing and intramolecular structure. *Macromolecules*, 36:260–267, 2003. doi:10.1021/ma0213495.

C. F. Abrams, L. Delle Site, and K. Kremer. Dual-resolution coarse-grained simulation of the bisphenol-a-polycarbonate/nickel interface. *Physical Review E*, 67:021807, 2003. doi:10.1103/PhysRevE.67.021807.

A. Agrios and P. Pichat. State of the art and perspectives on materials and applications of photocatalysis over $TiO_2$. *Journal of Applied Electrochemistry*, 35(7):655–663, July 2005. ISSN 0021-891X. doi:10.1007/s10800-005-1627-6.

C. Alliot, L. Bion, F. Mercier, and P. Toulhoat. Sorption of aqueous carbonic, acetic, and oxalic acids onto $\alpha$-alumina. *Journal of Colloid and Interface Science*, 287(2): 444–451, July 2005. ISSN 00219797. doi:10.1016/j.jcis.2005.02.043.

O. K. Andersen. Linear methods in band theory. *Physical Review B*, 12(8):3060–3083, October 1975. doi:10.1103/PhysRevB.12.3060.

R. Auhl, R. Everaers, G. S. Grest, K. Kremer, and S. J. Plimpton. Equilibration of long chain polymer melts in computer simulations. *The Journal of Chemical Physics*, 119 (24):12718–12728, 2003. doi:10.1063/1.1628670.

R. F. W. Bader. *Atoms in Molecules: A Quantum Theory*. Oxford University Press, New York, 1990.

S. R. Bahn and K. W. Jacobsen. An object-oriented scripting interface to a legacy electronic structure code. *Computing in Science & Engineering*, 4(3):56–66, 2002. doi:10.1109/5992.998641.

A. T. Bell. The impact of nanoscience on heterogeneous catalysis. *Science*, 299(5613): 1688–1691, March 2003. doi:10.1126/science.1083671.

H. J. C. Berendsen, D. van der Spoel, and R. van Drunen. Gromacs: A message-passing parallel molecular dynamics implementation. *Computer Physics Communications*, 91(1-3):43–56, September 1995. doi:10.1016/0010-4655(95)00042-E.

T. Björkman, A. Gulans, A. V. Krasheninnikov, and R. M. Nieminen. Van der Waals bonding in layered compounds from advanced first-principles calculations. *Physical Review Letters*, 108:235502, 2012. doi:10.1103/PhysRevLett.108.235502.

G. Blyholder. Molecular Orbital View of Chemisorbed Carbon Monoxide. *Journal of Physical Chemistry*, 68(10):2772–2777, Oct. 1964. ISSN 0022-3654. doi:10.1021/j100792a006.

P. E. Blöchl. Projector augmented-wave method. *Physical Review B*, 50(24):17953, 1994. doi:10.1103/PhysRevB.50.17953.

M. Born and J. Oppenheimer. Zur quantentheorie der molekeln. *Annals of Physics*, 389:457–484, 1927. doi:10.1002/andp.19273892002.

E. C. Botelho, R. A. Silva, L. C. Pardini, and M. C. Rezende. A review on the development and properties of continuous fiber/epoxy/aluminum hybrid composites for aircraft structures. *Materials Research*, 9(3):247–256, Sept. 2006. ISSN 1516-1439. doi:10.1590/S1516-14392006000300002.

J. Q. Broughton, F. F. Abraham, N. Bernstein, and E. Kaxiras. Concurrent coupling of length scale: Methodology and application. *Physical Review B*, 60(4):2391–2403, July 1999. doi:10.1103/PhysRevB.60.2391.

R. Car and M. Parrinello. Unified approach for molecular dynamics and density-functional theory. *Physical Review Letters*, 55(22):2471–2474, November 1985. doi:10.1103/PhysRevLett.55.2471.

S. D. Chakarova-Käck, Øyvind Borck, E. Schröder, and B. I. Lundqvist. Adsorption of phenol on graphite(0001) and $\alpha$-$Al_2O_3$(0001): Nature of van der Waals bonds from first-principles calculations. *Physical Review B*, 74:155402, October 2006. doi:10.1103/PhysRevB.74.155402.

P. G. de Gennes. Reptation of a Polymer Chain in the Presence of Fixed Obstacles. *The Journal of Chemical Physics*, 55(2):572, 1971. ISSN 00219606. doi:10.1063/1.1675789.

L. Delle Site, C. F. Abrams, A. Alavi, and K. Kremer. Polymers near metal surfaces: Selective adsorption and global conformations. *Physical Review Letters*, 89(15):156103, September 2002. doi:10.1103/PhysRevLett.89.156103.

L. Delle Site, A. Alavi, and C. F. Abrams. Adsorption energies and geometris of phenol on the (111) surface of nickel: An *ab initio* study. *Physical Review B*, 67:193406, 2003. doi:10.1103/PhysRevB.67.193406.

M. Dion, H. Rydberg, E. Schröder, D. C. Langreth, and B. I. Lundqvist. Van der Waals density functional for general geometries. *Physical Review Letters*, 92(24):246401+, Jun 2004. doi:10.1103/PhysRevLett.92.246401.

M. Dion, H. Rydberg, E. Schröder, D. C. Langreth, and B. I. Lundqvist. Erratum: Van der Waals density functional for general geometries [Phys. Rev. Lett. 92, 246401 (2004)]. *Physical Review Letters*, 95:109902, September 2005. doi:10.1103/PhysRevLett.95.109902.

J. Enkovaara, C. Rostgaard, J. J. Mortensen, J. Chen, M. Dułak, L. Ferrighi, J. Gavnholt, C. Glinsvad, V. Haikola, H. A. Hansen, H. H. Kristoffersen, M. Kuisma, A. H. Larsen, L. Lehtovaara, M. Ljungberg, O. Lopez-Acevedo, P. G. Moses, J. Ojanen, T. Olsen, V. Petzold, N. A. Romero, J. Stausholm-Møller, M. Strange, G. A. Tritsaris, M. Vanin, M. Walter, B. Hammer, H. Häkkinen, G. K. H. Madsen, R. M. Nieminen, J. K. Nørskov, M. Puska, T. T. Rantala, J. Schiøtz, K. S. Thygesen, and K. W. Jacobsen. Electronic structure calculations with GPAW: a real-space implementation of the projector augmented-wave method. *Journal of Physics: Condensed Matter*, 22 (25):253202+, June 2010. ISSN 0953-8984. doi:10.1088/0953-8984/22/25/253202.

C. Fonseca Guerra, J.-W. Handgraaf, E. J. Baerends, and F. M. Bickelhaupt. Voronoi deformation density (VDD) charges: Assessment of the Mulliken, Bader, Hirshfeld, Weinhold, and VDD methods for charge analysis. *J. Comput. Chem.*, 25(2):189–210, 2004. ISSN 1096-987X. doi:10.1002/jcc.10351.

T. J. Godin and J. P. Lafemina. Atomic and electronic structure of the corundum ($\alpha$-alumina) (0001) surface. *Physical Review B*, 49(11):7691, March 1994. doi:10.1103/PhysRevB.49.7691.

A. Gulans, M. J. Puska, and R. M. Nieminen. Linear-scaling self-consistent implementation of the van der Waals density functional. *Physical Review B (Condensed Matter and Materials Physics)*, 79(20):201105, 2009. doi:10.1103/PhysRevB.79.201105.

A. Gulans, A. Krasheninnikov, M. Puska, and R. Nieminen. Bound and free self-interstitial defects in graphite and bilayer graphene: A computational study. *Physical Review B*, 84(2):024114, July 2011. ISSN 1098-0121. doi:10.1103/PhysRevB.84.024114.

B. Hammer, L. Hansen, and J. Nørskov. Improved adsorption energetics within density functional theory using revised Perdew-Burke-Ernzerhof functionals. *Physical Review B*, 59:7413–7421, Mar 1999. doi:10.1103/PhysRevB.59.7413.

G. Henkelman, A. Arnaldsson, and H. Jonsson. A fast and robust algorithm for Bader decomposition of charge density. *Computational Materials Science*, 36(3):354–360, June 2006. ISSN 09270256. doi:10.1016/j.commatsci.2005.04.010.

B. Hess. P-lincs: A parallel linear constraint solver for molecular simulation. *J. Chem. Theory Comput.*, 4(1):116–122, January 2008. doi:10.1021/ct700200b.

B. Hess, S. Leon, N. Vegt, and K. Kremer. Long time atomistic polymer trajectories from coarse grained simulations: bisphenol-a polycarbonate. *Soft Matter*, 2(5):409–414, 2006. doi:10.1039/b602076c.

B. Hess, C. Kutzner, D. Vanderspoel, and E. Lindahl. Gromacs 4: Algorithms for highly efficient, load-balanced, and scalable molecular simulation. *J. Chem. Theory Comput.*, February 2008. doi:10.1021/ct700301q.

P. Hohenberg and W. Kohn. Inhomogeneous electron gas. *Physical Review*, 136(3B): B864–B871, Nov 1964. doi:10.1103/PhysRev.136.B864.

M. Hoikkanen, A. Luukkonen, J. Vuorinen, J. Blomqvist, K. Johnston, P. Salo, and R. Nieminen. Final report of Hybrid Products and in-Mold Integrated Structures. Technical report, Tampere University of Technology and Helsinki University of Technology, 2008.

K. Johnston, A. Gulans, T. Verho, and M. Puska. Adsorption structures of phenol on the Si(001)-(2x1) surface calculated using density functional theory. *Physical Review B*, 81(23):235428, June 2010. ISSN 1098-0121. doi:10.1103/PhysRevB.81.235428.

G. Kim and Y. Senda. A methodology for coupling an atomic model with a continuum model using an extended Lagrange function. *Journal of physics. Condensed matter : an Institute of Physics journal*, 19(24):246203, June 2007. ISSN 0953-8984. doi:10.1088/0953-8984/19/24/246203.

W. Kohn. Nobel Lecture: Electronic structure of matter - wave functions and density functionals. *Reviews of Modern Physics*, 71(5):1253–1266, Oct. 1999. ISSN 0034-6861. doi:10.1103/RevModPhys.71.1253.

W. Kohn and L. J. Sham. Self consistent equations including exchange and correlation effects. *Physical Review*, 140(4A):A1133–A1138, Nov 1965. doi:10.1103/PhysRev.140.A1133.

A. R. Leach. *Molecular Modelling: Principles and Applications*. Pearson Education Limited, 2nd edition, 2001. ISBN 0-582-38210-6.

K. Lee, E. D. Murray, L. Kong, B. I. Lundqvist, and D. C. Langreth. Higher-accuracy van der Waals density functional. *Physical Review B*, 82(8), 2010. doi:10.1103/PhysRevB.82.081101.

Y. Lei, F. Mehmood, S. Lee, J. Greeley, B. Lee, S. Seifert, R. E. Winans, J. W. Elam, R. J. Meyer, P. C. Redfern, D. Teschner, R. Schlogl, M. J. Pellin, L. A. Curtiss, and S. Vajda. Increased silver activity for direct propylene epoxidation via subnanometer size effects. *Science*, 328(5975):224–228, April 2010. doi:10.1126/science.1185200.

H. Limbach, a. Arnold, B. Mann, and C. Holm. ESPResSo-an extensible simulation package for research on soft matter systems. *Computer Physics Communications*, 174(9):704–727, May 2006. ISSN 00104655. doi:10.1016/j.cpc.2005.10.005.

E. Lindahl, B. Hess, and D. van der Spoel. Gromacs 3.0: a package for molecular simulation and trajectory analysis. *Journal of Molecular Modeling*, 7(8):306–317, 2001. doi:10.1007/s008940100045.

A. Luukkonen, E. Sarlin, M. Hoikkanen, M. Honkanen, M. Vippola, J. Vuorinen, T. Lepistö, T. Pärnänen, J. Blomqvist, M. Kanerva, V. Turkia, T. Brander, O. Saarela, P. Salo, and R. Nieminen. The final report of K3MAT: Light and Wear Resistant Hybrid Materials. Technical report, Tampere University of Technology and Aalto University, 2011.

A. Márquez, J. Graciani, and J. Sanz. Charge state of metal atoms on oxide supports: a systematic study based on simulated infrared spectroscopy and density functional theory. *Theoretical Chemistry Accounts: Theory, Computation, and Modeling (Theoretica Chimica Acta)*, 126(3):265–273, June 2010. ISSN 1432-881X. doi:10.1007/s00214-009-0703-0.

S. J. Marrink, A. H. de Vries, and A. E. Mark. Coarse grained model for semiquantitative lipid simulations. *The Journal of Physical Chemistry B*, 108(2):750–760, 2004. doi:10.1021/jp036508g.

S. J. Marrink, H. J. Risselada, S. Yefimov, D. P. Tieleman, and A. H. de Vries. The martini force field: Coarse grained model for biomolecular simulations. *The Journal of Physical Chemistry B*, 111(27):7812–7824, 2007. doi:10.1021/jp071097f. PMID: 17569554.

S. J. Marrink, M. Fuhrmans, H. J. Risselada, and X. Periole. The MARTINI Forcefield. In G. Voth, editor, *Coarse graining of condensed phase and biomolecular systems*, chapter 2, pages 1–21. CRC Press, 2008. URL `http://md.chem.rug.nl/~marrink/chapter2-voth08.pdf`.

R. M. Martin. *Electronic Structure: Basic Theory and Practical Methods*. Cambridge University Press, 2004.

H. J. Monkhorst and J. D. Pack. Special points for Brilliouin-zone integrations. *Physical Review B*, 13(12):5188, 1976. doi:10.1103/PhysRevB.13.5188.

L. Monticelli, S. K. Kandasamy, X. Periole, R. G. Larson, D. P. Tieleman, and S.-J. Marrink. The martini coarse-grained force field: Extension to proteins. *Journal of Chemical Theory and Computation*, 4(5):819–834, 2008. doi:10.1021/ct700324x.

J. J. Mortensen, L. B. Hansen, and K. W. Jacobsen. Real-space grid implementation of the projector augmented wave method. *Physical Review B*, 71(3):035109+, Jan 2005. doi:10.1103/PhysRevB.71.035109.

P. G. Moses, J. J. Mortensen, B. I. Lundqvist, and J. K. Nørskov. Density functional study of the adsorption and van der Waals binding of aromatic and conjugated compounds on the basal plane of $MoS_2$. *The Journal of Chemical Physics*, 130(10): 104709+, 2009. doi:10.1063/1.3086040.

M. Mura, A. Gulans, T. Thonhauser, and L. Kantorovich. Role of van der Waals interaction in forming molecule-metal junctions: flat organic molecules on the Au(111) surface. *Phys. Chem. Chem. Phys.*, 12(18):4759–4767, May 2010. ISSN 1463-9084. doi:10.1039/B920121A.

É. D. Murray, K. Lee, and D. C. Langreth. Investigation of Exchange Energy Density Functional Accuracy for Interacting Molecules. *Journal of Chemical Theory and Computation*, 5(10):2754–2762, Oct. 2009. doi:10.1021/ct900365q.

R. M. Nieminen. From atomistic simulation towards multiscale modelling of materials. *Journal of Physics: Condensed Matter*, 14(11):2859–2876, Mar. 2002. ISSN 0953-8984. doi:10.1088/0953-8984/14/11/306.

J. D. Pack and H. J. Monkhorst. Special points for Brillouin-zone integrations - a reply. *Physical Review B*, 16(4):1748, August 1977. doi:10.1103/PhysRevB.16.1748.

O. H. Pakarinen, J. M. Mativetsky, A. Gulans, M. J. Puska, A. S. Foster, and P. Grutter. Role of van der Waals forces in the adsorption and diffusion of organic molecules on an insulating surface. *Physical Review B*, 80(8):085401, 2009. doi:10.1103/PhysRevB.80.085401.

J. P. Perdew and W. Yue. Accurate and simple density functional for the electronic exchange energy: Generalized gradient approximation. *Phys. Rev. B*, 33:8800–8802, Jun 1986. doi:10.1103/PhysRevB.33.8800.

J. P. Perdew, J. Chevary, S. Vosko, K. A. Jackson, M. R. Pederson, D. Singh, and C. Fiolhais. Atoms, molecules, solids, and surfaces: Applications of the generalized gradient approximation for exchange and correlation. *Physical Review B*, 46(11):6671, 1992. doi:10.1103/PhysRevB.46.6671.

J. P. Perdew, K. Burke, and M. Ernzerhof. Generalized gradient approximation made simple. *Physical Review Letters*, 77:3865, 1996. doi:10.1103/PhysRevLett.77.3865.

J. P. Perdew, K. Burke, and M. Ernzerhof. Generalized gradient approximation made simple [phys. rev. lett. 77, 3865 (1996)]. *Physical Review Letters*, 78(7):1396+, Feb 1997. doi:10.1103/PhysRevLett.78.1396.

J. C. Phillips and L. Kleinman. New method for calculating wave functions in crystals and molecules. *Physical Review*, 116(2):287–294, October 1959. doi:10.1103/PhysRev.116.287.

M. Ramamoorthy, D. Vanderbilt, and R. D. K. Smith. First-principles calculations of the energetics of stoichiometric $TiO_2$ surfaces. *Physical Review B*, 49(23):16721–16727, Jun 1994. doi:10.1103/PhysRevB.49.16721.

G. Román-Pérez and J. M. Soler. Efficient implementation of a van der Waals density functional: Application to double-wall carbon nanotubes. *Physical Review Letters*, 103(9):096102+, Aug 2009. doi:10.1103/PhysRevLett.103.096102.

E. A. Rozhkova, I. Ulasov, B. Lai, N. M. Dimitrijevic, M. S. Lesniak, and T. Rajh. A high-performance nanobio photocatalyst for targeted brain cancer therapy. *Nano Letters*, 9(9):3337–3342, September 2009. ISSN 1530-6984. doi:10.1021/nl901610f.

M. Rubinstein and R. H. Colby. *Polymer Physics*. Oxford University Press, 2003.

E. Sanville, S. D. Kenny, R. Smith, and G. Henkelman. Improved grid-based algorithm for Bader charge allocation. *Journal of Computational Chemistry*, 28(5):899–908, April 2007. ISSN 01928651. doi:10.1002/jcc.20575.

T. Sinmazçelik, E. Avcu, M. O. Bora, and O. Çoban. A review: Fibre metal laminates, background, bonding types and applied test methods. *Materials & Design*, 32(7): 3671–3685, Aug. 2011. ISSN 02613069. doi:10.1016/j.matdes.2011.03.011.

J. M. Soler, E. Artacho, J. D. Gale, A. Garcia, J. Junquera, P. Ordejon, and D. Sanchez-Portal. The siesta method for ab initio order-n materials simulation. *Journal of Physics: Condensed Matter*, 14(11):2745–2779, 2002. doi:10.1088/0953-8984/14/11/302.

G. A. Somorjai. *Introduction to Surface Chemistry and Catalysis*. John Wiley & Sons, Inc., first edition, 1994. ISBN 0-471-03192-5.

G. Spoto, E. Gribov, G. Ricchiardi, A. Damin, D. Scarano, S. Bordiga, C. Lamberti, and A. Zecchina. Carbon monoxide MgO from dispersed solids to single crystals: a review and new advances. *Progress in Surface Science*, 76(3-5):71–146, October 2004. ISSN 00796816. doi:10.1016/j.progsurf.2004.05.014.

W. A. Steele. The physical interaction of gases with crystalline solids: I. gas-solid energies and properties of isolated adsorbed atoms. *Surface Science*, 36(1):317 – 352, 1973. ISSN 0039-6028. doi:10.1016/0039-6028(73)90264-1.

C. Su and D. L. Suarez. In sity infrared speciation of adsorbed carbonate on aluminum and iron oxides. *Clays and Clay Minerals*, 45(6):814–825, 1997.

W. Tang, E. Sanville, and G. Henkelman. A grid-based Bader analysis algorithm without lattice bias. *Journal of Physics: Condensed Matter*, 21(8):084204+, February 2009. ISSN 0953-8984. doi:10.1088/0953-8984/21/8/084204.

T. Thonhauser, V. R. Cooper, S. Li, A. Puzder, P. Hyldgaard, and D. C. Langreth. Van der Waals density functional: Self-consistent potential and the nature of the van der Waals bond. *Physical Review B*, 76(12):125112, Sept. 2007. ISSN 1098-0121. doi:10.1103/PhysRevB.76.125112.

A. Tkatchenko and M. Scheffler. Accurate Molecular Van Der Waals Interactions from Ground-State Electron Density and Free-Atom Reference Data. *Physical Review Letters*, 102(7):6–9, Feb. 2009. ISSN 0031-9007. doi:10.1103/PhysRevLett.102.073005.

N. Troullier and J. L. Martins. Efficient pseudopotentials for plane-wave calculations. *Physical Review B*, 43(3):1993–2006, January 1991. doi:10.1103/PhysRevB.43.1993.

D. Van Der Spoel, E. Lindahl, B. Hess, G. Groenhof, A. E. Mark, and H. J. Berendsen. Gromacs: fast, flexible, and free. *J Comput Chem*, 26(16):1701–1718, December 2005. ISSN 0192-8651. doi:10.1002/jcc.20291.

D. Vanderbilt. Soft self-consistent pseudopotentials in a generalized eigenvalue formalism. *Physical Review B*, 41(11):7892, 1990. doi:10.1103/PhysRevB.41.7892.

C. A. J. R. Vermeeren. An Historic Overview of the Development of Fibre Metal Laminates. *Applied Composite Materials*, 10:189–205, 2003. doi:10.1023/A:1025533701806.

O. A. Vydrov and T. Van Voorhis. Nonlocal van der Waals density functional: the simpler the better. *The Journal of chemical physics*, 133(24):244103, Dec. 2010. ISSN 1089-7690. doi:10.1063/1.3521275.

J. Wellendorff, A. Kelkkanen, J. Mortensen, B. Lundqvist, and T. Bligaard. RPBE-vdW description of benzene adsorption on Au(111). *Topics in Catalysis*, 53:378–383, February 2010. ISSN 1022-5528. doi:10.1007/s11244-010-9443-6.

Z. Xu, F. S. Xiao, S. K. Purnell, O. Alexeev, S. Kawi, S. E. Deutsch, and B. C. Gates. Size-dependent catalytic activity of supported metal clusters. *Nature*, 372(6504): 346–348, November 1994. ISSN 0028-0836. doi:10.1038/372346a0.

Y. Zhang and W. Yang. Comment on "generalized gradient approximation made simple". *Physical Review Letters*, 80(4):890+, Jan 1998. doi:10.1103/PhysRevLett.80.890.

Aalto-DD 114/2012

ISBN 978-952-60-4774-4
ISBN 978-952-60-4775-1 (pdf)
ISSN-L 1799-4934
ISSN 1799-4934
ISSN 1799-4942 (pdf)

**Aalto University**
**School of Science**
**Department of Applied Physics**
**www.aalto.fi**

BUSINESS + ECONOMY

ART + DESIGN + ARCHITECTURE

SCIENCE + TECHNOLOGY

CROSSOVER

**DOCTORAL DISSERTATIONS**